Solvation Ultrafast Dynamics of Reactions. 12. Probing along the Reaction Coordinate and Dynamics in Supercritical Argon

Arnulf Materny,[†] Christoph Lienau,[‡] and Ahmed H. Zewail*

Arthur Amos Noyes Laboratory of Chemical Physics, California Institute of Technology, Pasadena, California 91125

Received: August 9, 1996; In Final Form: September 23, 1996[⊗]

In this paper, our focus is on the influence of the solvent density on the caging, recombination dynamics, and the nature of the reaction coordinate of iodine in supercritical argon at pressures of 0−2500 bar. Femtosecond probing with widely tunable pulses allows us to directly resolve the geminate recombination of iodine atoms and the subsequent relaxation processes. A nonzero recombination yield is found at argon pressures as low as 200 bar, and this yield increases strongly with increasing solvent density. The mechanism involves recombination onto the A/A′ states. At high pressures, a large fraction of the iodine atoms undergo an ultrafast "in-cage" recombination which is measured on the subpicosecond time scale at 2500 bar of argon. In addition, a fraction of the iodine atoms break through the solvent cage and begin a diffusive motion through the rare-gas solvent. Experimental evidence is presented and indicates that this diffusive motion leads to reencounters and subsequent recombination of the geminate iodine pair. This diffusive recombination occurs on a significantly longer time scale than the rapid "in-cage" recombination. The newly-formed iodine molecules undergo vibrational relaxation within the A/A′ state, and the dynamics of this process and its dependence on the solvent density are revealed. A key concept here is the solvent density-induced control of the rigidity of the first solvent shell surrounding the dissociating iodine atoms. As shown before [Liu et al. *Nature* **1993**, *364*, 427], such studies of solvation present a unique opportunity of examining the microscopic influence of the solvent structure on reaction dynamics in clusters and solutions.

I. Introduction

In the preceding paper,[1] we presented studies of the reaction dynamics of iodine in rare-gas solvents: helium, neon, argon, and krypton. Of particular interest was the dynamics of bond breakage, wave packet dephasing, and changes in the potential energy surfaces as the liquid density regime was reached. In this paper, we focus our attention on the dynamics and state of atoms recombination. We determine the state of recombination by probing the motion along the reaction coordinate at different internuclear separations.

Studies of the recombination of a pair of atoms, which constitutes one of the most fundamental processes in condensed-phase chemistry, have been pursued over the past 60 years. As early as 1934, Franck and Rabinowitch[2] outlined a mechanism that may describe the recombination process that follows the photodissociation of iodine in solution. They proposed that the atoms which are formed in the dissociation will rapidly lose their excess kinetic energy through collisions with the surrounding solvent molecules and then recombine at a short distance from their former partners. Thus, the probability for this *geminate* pair to recombine after the dissociation process will be enhanced in a three-body collision with a solvent molecule. This recombination of two atoms imprisoned inside a solvent "cage" has been termed "primary" recombination, in order to distinguish it from the ordinary *nongeminate* recombination of atoms randomly distributed within the solvent.[3]

Subsequent studies by Noyes and co-workers provided the first quantitative measurements of the quantum yield for geminate recombination of iodine[4] and of its dependence on the viscosity of the solvent[5] as well as on the wavelength of the dissociating light.[6] Noyes also introduced a classification of the two different possible recombination pathways. *Primary recombination* designates only those processes where the fragments recombine within a solvent "cage" without reaching a separation of more than one molecular diameter. This is clearly a rapid and nondiffusive process which is sensitive to the local structure of the solvent around the parent iodine molecule and thus to short-range iodine−solvent interactions. The second pathway, *secondary recombination*, corresponds to fragments originating from the *same* parent molecule that reencounter during a diffusion process and form a new molecule. If the fragments are able to break out of the solvent cage, they begin a random diffusion through the solvent. Both primary and secondary caging correspond to *geminate* recombination processes. Accordingly, the much slower diffusive recombination of fragments from different parent molecules is termed *nongeminate*.

Laser flash photolysis experiments[7,8] provided kinetic studies relevant to the recombination mechanism. With photolysis, the groups of Troe[9−13] and van den Bergh[14,15] provided accurate measurements of the quantum yields for geminate recombination and of the rate coefficients for the nongeminate recombination in a large number of solvents under conditions ranging from low-pressure gases to high-pressure liquids. These results were consistently explained in terms of diffusion models.[16] Due to the low time resolution, however, these experiments could not provide detailed information about the primary steps of bond breakage and re-formation. The experimental and theoretical studies have been reviewed in the preceding paper.

[†] Deutsche Forschungsgemeinschaft Postdoctoral Fellow. Present address: Institut für Physikalische Chemie der Universität Würzburg, Marcusstr. 9-11, D-97070 Würzburg, Germany.

[‡] Deutsche Forschungsgemeinschaft Postdoctoral Fellow. Present address: Max-Born-Institut für Nichtlineare Optik und Kurzzeitspektroskopie, Rudower Chaussee 6, D-12489 Berlin, Germany.

[⊗] Abstract published in *Advance ACS Abstracts,* November 1, 1996.

S0022-3654(96)02431-8 CCC: $12.00

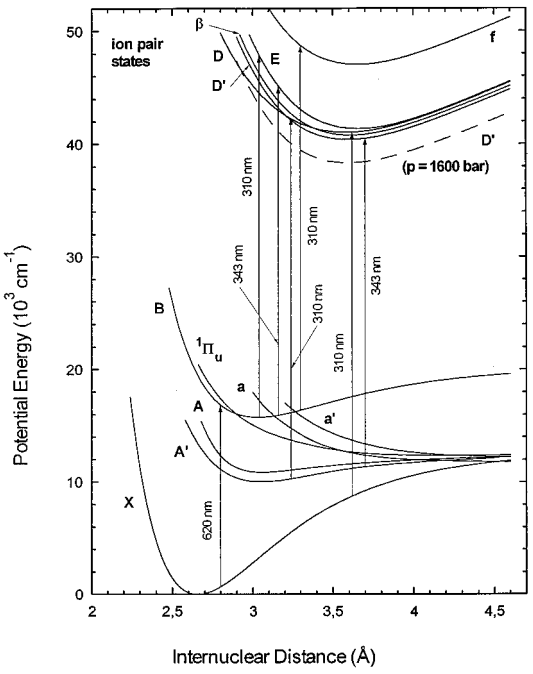

Figure 1. Potential energy curves of I_2 relevant for the present study. Six of the ten states correlating with ground-state atoms are shown. Solid lines designate gas-phase potentials (see text for references). The dashed line shows the solvent shift of the D' ion pair state in argon at 1600 bar and 293 K, as approximated from the solvent shift on the D′ → A′ fluorescence emission. Vertical arrows indicate optical transitions used to excite (620 nm) and to probe the dissociation and recombination dynamics of iodine in supercritical rare-gas solvents.

Here, using a 60 fs laser, centered at 620 nm, we excite iodine mostly to low vibrational levels in the bound B state. We then probe the evolution of the prepared wave packet using a ∼100 fs probe pulse with wavelengths that were continuously tunable from 275 to 400 nm. The goal is to resolve the different elementary reaction steps involved in the recombination and to test the microscopic model for caging and, its precursor, the dissociation process. Such findings and concepts of the role of coherence and its time scale are directly relevant to the interpretation of recent picosecond experiments in liquids, high-pressure gases, clusters, and rare-gas matrices. We also examined vibrational relaxation in the A/A′ states, a process that is important for nonadiabatic caging on the ground state.

There are various, compelling reasons why compressed rare gases constitute an especially appealing class of solvents to be studied.[17−19] First and foremost, a continuous change of solvent pressure allows us to gradually vary the properties of the solvent, from an essentially ideal gas, with mean durations between collisions that exceed the time scale of our experiments, to a liquidlike superfluid at the highest pressures reached in our study (2500 bar); the mean time between collisions as a function of density is given in Figure 2 of the preceding paper. Variation of the pressure of a supercritical gas thus provides a means to gradually vary the solute−solvent interaction over an extremely wide range. Second, lowering the pressure makes it possible to gradually loosen the rigidity of the solvent cage and hence increase the probability for escape out of the cage. It should, therefore, be possible to increase the relative contribution of the secondary recombination, a process that was not verified experimentally. Finally, the potentials for the rare-gas solvents are easier to construct and provide grounds for direct comparisons with theory and with molecular dynamics simulations.

The paper is outlined as follows. After the preliminaries in section II, we briefly discuss the experimental arrangement in section III. Section IV gives the results, and section V the discussion. In section VI we summarize our findings.

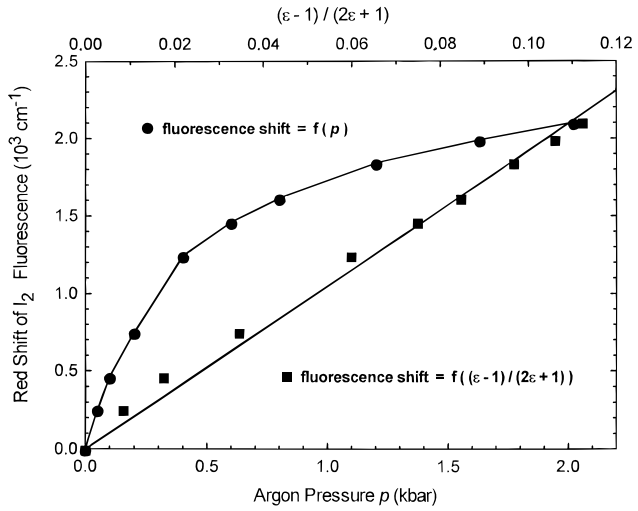

Figure 2. Experimentally observed solvent-induced red shift of the D′ → A′ fluorescence emission of iodine in argon at pressures between 0 and 2000 bar.

II. Preliminaries

In this section, we will introduce the spectroscopic information that is relevant for the studies made here. This includes a brief discussion of the iodine gas-phase potentials and of the solvent effect on these potentials. Briefly, we will review our earlier experiments on iodine but with particular focus on supercritical argon.

In Figure 1 we show a sketch of the electronic potential energy curves that are discussed here. The potential energy curves of the ground $X0_g^+(^1\Sigma)$[20] and excited $B0_u^+(^3\Pi)$ state are known from high-resolution Fourier transform spectroscopy[21] and from coherent wave packet spectroscopy.[22,23] The results of the studies are usually given in terms of a Dunham expansion,[24] from which accurate potential energy curves can be obtained either by RKR inversion[25−28] or by fitting of the spectroscopic constants to parametrized potential functions.[29,30] Besides the X state, there are nine more states that correlate with ground-state iodine atoms. The potentials of six of them are experimentally known, i.e. the weakly bound $A'2_u(^3\Pi)$[31] and $A1_u(^3\Pi)$[32] and the repulsive $0_u^+(^3\Pi)$,[32] $a1_g(^3\Pi)$,[33,34] $B''1_u(^1\Pi)$,[33] and $a'0_g^+(^3\Sigma^-)$.[35] This leaves only three of the ten Hund's case (c) states, which correlate with ground state iodine atoms, experimentally unknown. All of them are supposed to be repulsive.

The ion-pair states of iodine, which are a topic of current interest,[36−38] show a clear clustering of electronic term values into three groups, with energy spacings close to that between the term values of the $^3P_2$, $^3P_1/^3P_0$, and $^1D_2$ atomic ion states.[36] Fourteen out of the 20 ion-pair states that correlate with the manifold of $I^+ + I^-$ atomic ion states have been identified experimentally. Of particular relevance to our experiments are those belonging to the energetically lowest lying group. These are the states $D'2_g$,[31] $\beta 1_g$,[39] $D0_u^+$,[40] $E0_g^+$,[41] $\gamma 1_u$,[42] and $\delta 2_u$.[42] All of these states are very close in energy and are assumed to undergo extensive mixing in liquids or high-pressure gases. Furthermore, one of the states of the second cluster $f0_g^+$ [43] needs to be considered here.

The potential energy curves of the iodine valence states in solution differ only slightly from their gas-phase potentials. This was quantified in the preceding paper and is apparent from resonance Raman experiments,[44] as well as from spectroscopic

studies in large clusters and in rare-gas matrices.[45] In contrast, the ion-pair states are known to be strongly affected by the solvent, due to the strong solvation of the molecular dipole of iodine in the ion-pair states by the dielectric of the solvent. This solvent effect becomes most apparent in the strong red shift of the D′ → A′ fluorescence emission, which is centered at 342 nm in low-pressure rare gases.[46] In argon at high pressures, we observe a shift in the center wavelength of this transition from 342 nm at 0 bar to 368 nm at 2000 bar, which corresponds to a solvation energy of about 2000 cm^{-1}. The red shift should be compared to the solvent shift in large Ar_n clusters,[45] where the intensity maximum of the transition is shifted to ∼400 nm (corresponding to a solvation energy of 4240 cm^{-1}), and in low-temperature argon matrices, where a relatively smaller shift to 380 nm (or 2920 cm^{-1})[46] is observed.

As mentioned in the preceding paper, the observed shifts are evidently due to solvation of the molecular dipole of iodine, in the ion-pair states, and can, to a first approximation, be accounted for by the classical cavity cell model.[47,48] The assumption is one of a nonpolarizable point dipole isolated in the center of a cavity in a uniform dielectric medium. The spectral shift in energy is then given by [49]

$$\Delta E = \frac{\epsilon - 1}{2\epsilon + 1}\frac{\Delta(\mu^2)}{a^3} \qquad (1)$$

where ϵ is the static dielectric constant of the solvent (for argon at high pressure see ref 50), $\Delta(\mu^2)$ is the difference in the squares of the ground- and excited-state dipole moments, and a is the diameter of the cavity, which we assume to be pressure independent. As shown in Figure 2, we could experimentally verify the linear relationship between the solvent-induced red shift ΔE of the D′ → A′ transition and $(\epsilon - 1)/(2\epsilon + 1)$, as suggested by eq 1, for argon. In the preceding paper, Figure 5 gives this behavior for different solvents including argon.

If we excite ground-state iodine molecules with a 60 fs laser pulse centered at 620 nm, nearly 62% of the molecules reach vibrational levels $v' = 6-11$ of the bound B state[22] (centered around $v' = 8$), while 34% of the molecules are placed on the weakly bound A state and the remainder on the dissociative $^1\Pi$ state.[51] The dynamics of the prepared wave packet are then interrogated by a second pulse, e.g., centered at 310 nm, and this probe pulse can excite B state molecules to either the $f0_g^+$ [52,53] or $E0_g^+$ [54,55] ion-pair states. In our experiments, we detect the ion-pair state fluorescence as a function of the delay time between pump and probe pulses. In the presence of argon buffer gas, the initially excited ion-pair state population rapidly relaxes into the lowest vibrational levels of $D'2_g$, which is the lowest energy ion-pair state. This relaxation is so fast that, under our conditions ($p \geq 10$ bar), the fluorescence emission spectrum after two-photon absorption is entirely dominated by the very intense D′ → A′ emission.

In the absence of argon, the wave packet created by the pump pulse freely propagates on the B state potential.[22,23,29] The period(s) of the oscillatory motion of this wave packet was first observed under collisionless conditions and showed manifestations of anharmonicity which leads to an interference pattern on the laser-induced fluorescence (LIF) signal with a recurrence period of about 9 ps (see Figure 3). In this case, the lifetime of the B state wave packet is on the order of microseconds, reaching the B state radiative decay (lifetime τ_0).[56−58] Addition of a buffer gas leads to a solvent-induced dephasing of this wave packet by predissociation and vibration−rotation coupling, as detailed in the preceding paper.

The repulsive state populated by predissociation has not been conclusively identified, but it is likely to be either the $a1_g(^3\Pi)$ or $a'0_g^+(^3\Sigma^-)$ state. This problem has been the topic of a recent resonance Raman study[59] by the groups of Schwentner and Chergui. Both states cross the B state at low energies; $a1_g(^3\Pi)$ crosses near the outer turning point of $v' = 1$ and $a'0_g^+(^3\Sigma^-)$ near $v' = 5$. The decays observed using pump−probe pulses in high-pressure argon (Figure 3) reflect this predissociation process. The predissociation rate is found to increase linearly with density and reaches 1.1 ps^{-1} at 2500 bar. These rates differ from the reported predissociation rate of 4.4 ps^{-1} in *n*-hexane measured by Scherer et al.[60,61] Furthermore, the interpretation of these rates in terms of the Stern−Volmer model, rewritten to include the density, yields a quenching cross section of 11.1 $Å^2$,[1] which is remarkably close to the one obtained by Capelle and Broida[62] in argon at pressure of 4×10^{-5} bar and at an excitation wavelength of 620 nm. From this we conclude that the same predissociation mechanism is active in dilute and dense gases at liquidlike densities. The transients in Figure 3 also reveal the persistence of coherent motion of the B state wave packet for more than 1.5 ps at pressures as high as 800 bar, and this aspect has been addressed in the preceding paper.

At very high pressures, the decay in the LIF signal is followed by a slower rise. This rise is attributed to molecules recombining geminately on the weakly bound A or A′ state surfaces. In order to support this interpretation, we present here a series of experiments in which we vary the wavelength of the probe laser from 275 to 400 nm at different pressures of argon. Before

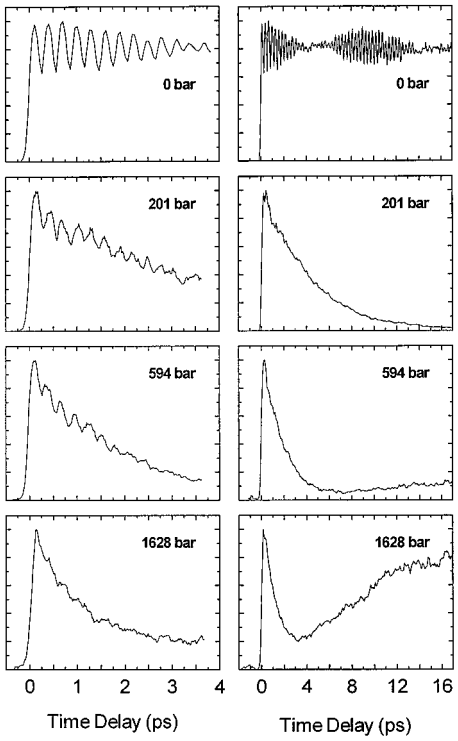

Figure 3. Femtosecond transients of iodine in compressed supercritical argon at 293 K at pressures of 0, 201, 594, and 1628 bar and on two time scales. Experiments have been recorded using LIF detection at "magic" angle polarization between pump (620 nm) and probe (310 nm) wavelengths. Detection wavelength was varied with pressure to optimize LIF signal. Note the persistence of coherent vibrational motion of the B state wave packet for 2 ps at a pressure of 594 bar. The initial peak on the first oscillation reflects the direct dissociation of the fraction of molecules that is excited onto the repulsive A state. The 15 ps transients indicate the increase in B state predissociation rate with increasing pressure. At 1600 bar, the rise in signal intensity at delay times longer than 4 ps reflects the geminate recombination of iodine atoms and the subsequent vibrational relaxation within the A/A′ states. Except for the 0 bar data, the step size used in this transient was too large to resolve the coherent wave packet motion.

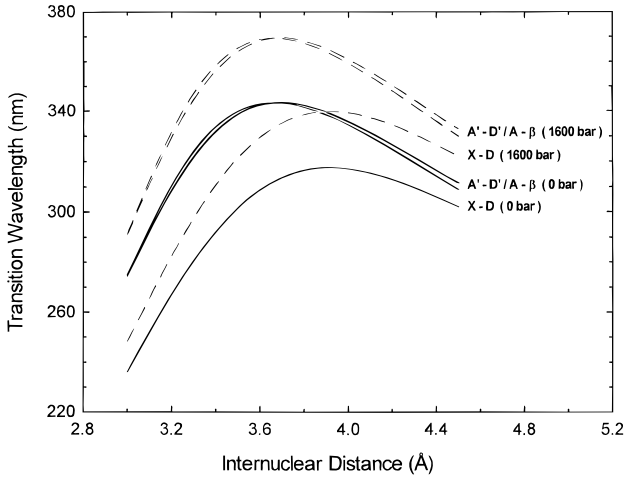

Figure 4. Difference potentials for isolated gas-phase iodine molecules (solid line) and iodine in argon at 1600 bar and 293 K (dashed line). In high-pressure argon, all iodine ion-pair states have been assumed to be lowered in energy by an amount ΔE. This decrease in energy has been obtained from the experimentally observed red shift in the D′ → A′ fluorescence emission spectrum (see Figure 3) and was assumed to be independent of internuclear distance.

discussing the results of these experiments, we will qualitatively predict the electronic states of iodine that might be involved in the absorption of a photon in this wavelength region. Since geminate recombination leads to the formation of iodine molecules on three different electronic states, X, A, and A′, we need to consider the following optical transitions to ion-pair states of the first group: X → D, A → β, A′ → D′. Due to strong coupling between the ion-pair states in high-pressure rare gases, all transitions are expected to lead to the same emission, namely, emission from the vibrationally relaxed lowest ion-pair state: D′ → A′.

The following discussion of the absorption from these states is based on the classical Franck principle.[63] It states that both nuclear positions and momenta of a molecule remain unchanged during the absorption of a photon, and this implies that the kinetic energy of a particle is conserved during the transition. For diatomic molecules, in this classical picture, this means that all molecules at a given internuclear distance absorb light at the same wavelength, even though their kinetic energy may vary. The absorption wavelength is then given by the energy difference between the potential energy surfaces of the two electronic states involved in the transition (Mulliken's difference potentials[64,65]). The difference potentials for isolated gas-phase I_2 molecules are given in Figure 4. It can be seen that a laser pulse centered at 310 nm can be absorbed by molecules in all three electronic states, X, A, and A′. The diagram also shows that ground-state molecules can absorb the photon only at internuclear distances much larger than the equilibrium X state distance of 2.67 Å, corresponding to high vibrational levels with $E_{vib} \geq 5000$ cm^{-1}.

Molecules in the A or A′ state, however, can absorb at large internuclear distances as well as at distances close to the equilibrium distance of 3.06 and 3.08 Å, respectively. Tuning the probe laser further to the red (350 nm), X state molecules can no longer absorb the pulse; the entire absorption originates from molecules in the A or A′ states at internuclear distances significantly larger than the equilibrium distance. We should thus be able, by tuning the probe laser to the red, to obtain a LIF signal that comes *exclusively* from molecules in high vibrational levels of the A or A′ states. The same argument holds in the presence of argon buffer gas. In this case we estimate the difference potentials by assuming a decrease in the potential energy of the ion-pair state that is independent of internuclear distance. We assume below that this solvation energy is given by the pressure-dependent red shift of the center wavelength of the D′ → A′ transition (see Figure 2). This is certainly a crude estimate, which should be further refined, for example, by including the dependence the of ion-pair state dipole moment on internuclear distance. We believe, however, that these refinements do not alter the qualitative discussion that follows. Under these assumptions, a 310 nm laser pulse still probes molecules on all three electronic states.

Whereas the short internuclear distances at which the A/A′ states are probed are only slightly dependent on pressure (see Figure 4), we notice a more significant change on the ground-state internuclear distances (e.g., 3.65 Å at 0 bar → 3.4 Å at 1600 bar), equivalent to probing more and lower vibrational levels in the ground state. Also, both the ground state and A/A′ state absorption should shift to the red. We observe a "cutoff" wavelength of 345 nm at 1600 bar vs 315 nm at 0 bar for the ground state and a similar red shift from 348 nm at 0 bar to 365 nm at 1600 bar for the A/A′ states. The difference in these "cutoff" wavelengths for the X and A/A′ state is significant (~30 nm). Thus, even taking into account the broad laser bandwidth (fwhm of 10 nm) and the dependence of the ion-pair state potential energy surfaces on solvent fluctuations, the absorption at red wavelengths should be entirely dominated by molecules on the A or A′ states. With this in mind, we should be able to separate the recombination and subsequent vibrational relaxation dynamics on the A/A′ states from those on the electronic ground state and clarify the geminate recombination mechanism in compressed rare gases. The absorption spectra of the D′ ← A′ and β → A transitions are expected to be so similar that, considering the spectral resolution of our lasers and the inherent spectral congestion in high-pressure gases, we will not be able to distinguish between absorptions from both these states.

III. Experimental Section

The 60 fs laser pulses centered at 620 nm, with a repetition rate of 100 MHz and a pulse energy of 20 pJ, were generated from a home-built colliding-pulse mode-locked ring dye laser (CPM). The CPM laser that consists of a gain jet (Rhodamine 6G/ethylene glycol), a saturable absorber jet (DODCI/ethylene glycol), seven single stack dielectric mirrors, and four quartz prisms is pumped by a multiline CW argon ion laser (Coherent Innova 310 with PowerTrack) running at ~3 W (see Figure 5). The 20 pJ output pulses of the CPM were amplified to more than 1.5 mJ in a four-stage dye amplifier pumped by the second harmonic of a 30 Hz Nd:YAG laser (Spectra Physics GCR 4A). Sulforhodamine B dye dissolved in water was used in the first amplifier stage, while Rhodamine 640/water was used in the last three stages. Amplified spontaneous emission was reduced by spatial filters after stages 1 and 3 and a saturable absorber jet (Malachite Green/ethylene glycol) after stage 2.

While the first three stages were pumped transversally, the fourth stage was a longitudinally pumped double-pass cell, and the YAG profile in this cell was expanded to a diameter of 1 cm. The output pulses were recompressed in a double-pass two-prism sequence to a pulse width of 60 fs fwhm (assuming a Gaussian pulse profile) and then split by a 50/50 dichroic beam splitter into the pump and probe arm of a Michelson interferometer. In the probe arm, 310 nm pulses with a pulse duration of 60 fs were generated by frequency-doubling the attenuated red pulses in a 1 mm KDP crystal. All other probe wavelengths were obtained by focusing the amplified red pulses into a water cell to generate a white light continuum, from which a particular wavelength was selected using a 10 nm fwhm interference filter.

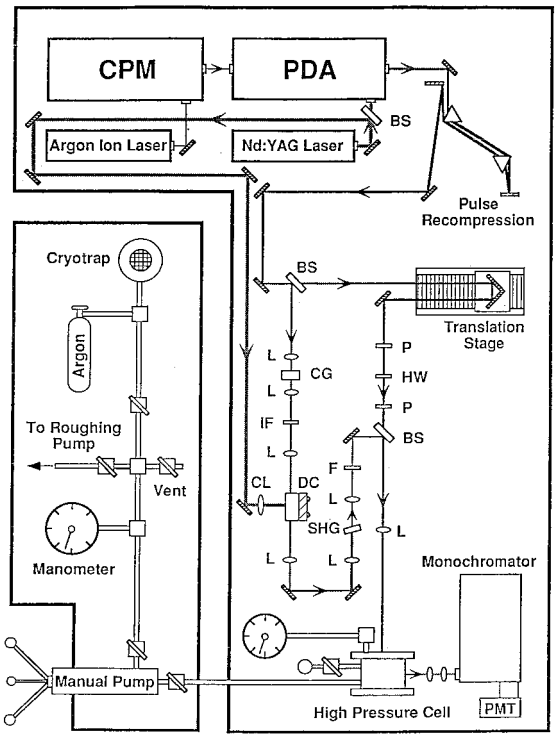

Figure 5. Overall schematic of the experimental setup used in the high-pressure studies. Key: CPM, colliding-pulse mode-locked dye laser; PDA, four-stage pulsed dye amplifier; BS, beam splitter; CL, cylindrical lens; L, lens; CG, continuum generation (water cell); IR, interference filter; DC, one-stage dye amplifier; SHG, second-harmonic generation crystal; F, filter; P, polarizer; HW, half-wave plate; PMT, photomultiplier tube.

These pulses were amplified in a single-pass dye amplifier stage, transversally pumped by residual 532 nm YAG output.

The desired wavelength in the UV was obtained by frequency-doubling in a 1 mm KDP crystal. These UV pulses, tunable from 275 to 400 nm, had a pulse duration of less than 150 fs and a spectral width of 8 nm and were directly used without recompression. The pump beam passed through two polarizers and a half-wave plate to allow variation in the relative polarization of pump and probe lasers. The angle between pump and probe polarizations was kept constant at 54.7°, although this angle may not be the perfect magic angle.[66] Studies of the rotational anisotropy at high pressures will be discussed elsewhere.

The pump and probe lasers were overlapped by means of a dielectric beam splitter and were focused slightly beyond the output window of the high-pressure cell in order to prevent white light continuum generation. Laser-induced fluorescence was collected at right angles to the laser propagation direction, collimated into a 20 cm, computer-controlled monochromator, and detected with a photomultiplier tube (PMT). The slit width of the monochromator was kept at 2 mm, which corresponds to a spectral width of 6 nm (fwhm). The fluorescence signal from the PMT was averaged in a boxcar integrator and recorded as a function of delay between the pump and probe pulses. This delay was controlled using a high-precision computer-controlled actuator that allowed for optical delays of up to 1 ns with a minimal step size of 0.7 fs. Five data points were accumulated at each actuator position. In a typical experimental scan, data were recorded at 200−400 different actuator positions. The scans were repeated until the desired signal-to-noise ratio was achieved, which required, in general, 10−80 scans. Data were analyzed using standard software (MINSQ), which allows one to account for the finite width of the laser pulses and a self-written fitting program (see ref 67) based on a Levenberg−Marquardt nonlinear least-squares algorithm. A description of the fitting procedure will follow in section V.

The home-built high-pressure cell was constructed from heat-treated stainless steel (Vascomax 300, tensile strength 300 000 psi). Four optical windows (diameter 6 mm, clear aperture 2 mm) were centered in each of the four walls. The input window is 4.0 mm thick quartz, while the output and fluorescence collection windows are 2.8 mm thick sapphire. Quartz windows are advantageous in that they reduce the temporal dispersion of the femtosecond pulses. The pressure in the cell was constantly monitored with a high-precision strain gauge pressure transducer, and the temperature inside the cell could be measured with a commercial high-pressure thermocouple. The distance between input and output windows was chosen at 6 mm, so that the total cell volume was limited to 0.2 cm^3. Such a small cell volume is essential because it allows, even in the case of rare gases, the use of a small, manually operated, screw-type pressure generator. Pressure inside the cell was generated by flushing argon into the preevacuated cell and manually compressing it to the desired pressure in an iterative process. To reach pressures above 1200 bar, argon gas had to be precompressed to 300 bar by liquefication in a pressure-resistant cryotrap. The cell showed no decrease in argon pressure (less than 1 bar) during the course of an experiment.

IV. Results

In this section, we present the results obtained from a series of experiments in compressed supercritical argon at a temperature of 293 K and at pressures ranging from 100 to 2500 bar. Ground-state iodine molecules were excited with 620 nm, 60 fs pulses. The probe wavelength was varied from 275 to 400 nm. The fluorescence detection wavelength in each of these experiments was chosen in order to maximize the D′ → A′ fluorescence signal and to avoid overlap with scattered probe laser light. A possible constant background on all of these transients was evaluated by averaging over fluorescence signal intensities at negative delay times and subsequently subtracted from the data. The signal amplitude of each transient was normalized to the intensity maximum of the B state laser-induced fluorescence at early times; in the following, all amplitudes will be given relative to this B state maximum. Furthermore, in each transient, time zero was fixed to the time at which the signal intensity on the initial rise at early times reaches 50% of the maximum B state fluorescence intensity (or an amplitude of 0.5). At each pressure we recorded scans over four different time intervals (if not otherwise noted: 4, 30, 200, and 800 ps, corresponding to time delays of 20 fs, 133 fs, 667 fs, and 2.67 ps between adjacent data points). We will now discuss these transients.

At a pressure of 100 bar of argon, the signal (Figure 6), observed on a 200 ps scan (0.67 ps/point) shows an exponential decay with a time constant of 8 ps. This decay is independent of the probe wavelength and the fluorescence detection wavelength and reflects the decay of the excited B state population due to collision-induced electronic predissociation.[1] We could not detect a fluorescence signal after the B state was completely depopulated, and we thus conclude that, at this pressure, the geminate recombination probability is so low that the signal from recombined molecules was not detected. If the transient was scanned with increased time resolution (see preceding paper), we observed a damped oscillatory modulation of the fluorescence signal, which reflects the dephasing of the coherent vibrational motion of the wave packet. The transient also shows the ultrafast dissociation of molecules excited onto the repulsive

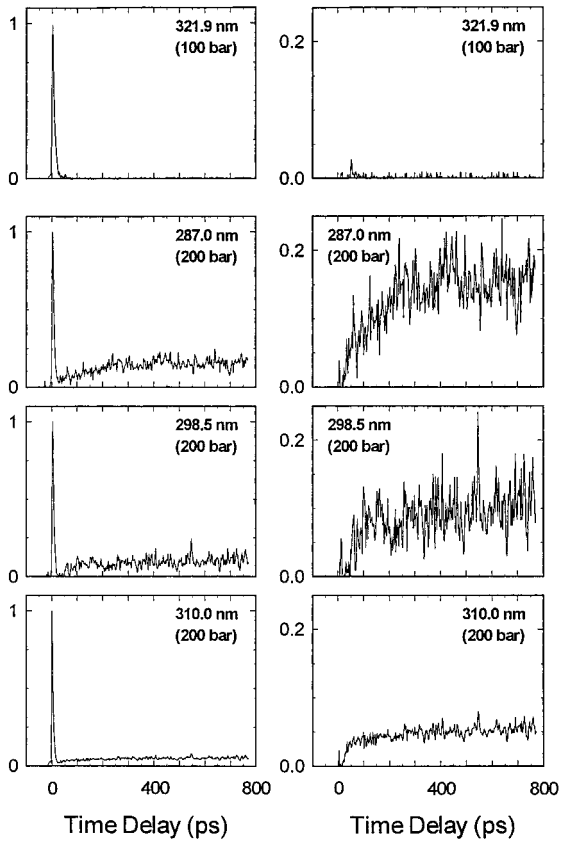

Figure 6. Transients of iodine in compressed supercritical argon at pressures of 100 and 200 bar on a time scale of 800 ps (2.67 ps/data point). The left column shows the original data while the right column shows the transients after subtraction of the B state fluorescence. Experiments have been recorded at a temperature of 293 K using LIF detection at "magic" angle polarization between the pump (620 nm, 60 fs) and probe (variable wavelength, less than 150 fs) pulses. The detection wavelength was varied with pressure and probe wavelength in order to optimize D′ → A′ fluorescence emission and minimize overlap with scattered probe laser light. No dependence of the transients on the detection wavelength could be observed. The signal amplitudes are normalized to the maximum in B state fluorescence intensity. The observation of fluorescence from iodine molecules in the A/A′ state indicate the onset of geminate recombination of atomic iodine in argon at a pressure of 200 bar.

A state branch at very early times (<150 fs). Within the first 3 ps, the B state signal that is underlying the oscillatory modulation shows a nonexponential decay, which might relate to vibrational relaxation within the B state.

At 200 bar (Figure 6), the initial decay of the B state population occurs at a rate of 0.25 ps^{-1} and is followed by a slow rise in fluorescence intensity. In the probe wavelength range from 277.5 to 310 nm, the maximum amplitude of this rising signal, termed "recombination signal", corresponds to about 5% of the maximum B state intensity at early times. If we tune the probe wavelength further to the red, its amplitude decreases. In the range from 277.5 to 310 nm, the form of the recombination signal is insensitive to the actual wavelength of the probe laser. The total fluorescence signal decreases to zero after about 20 ps (the B state is depopulated) and starts to rise again only after 35−40 ps. The recombination signal reaches its maximum intensity after about 200 ps, and we estimate a rise time (assuming a single-exponential rise) of about 60 ps. The intensity of the recombination signal is found to remain constant for delay times between 200 and 800 ps.

Increasing the pressure by another factor of 2 to 400 bar (Figure 7a,b) leads to qualitatively similar transients at UV probe wavelengths from 275 to 310 nm. The B state decay rate increases in proportion to the change in density to 0.45 ps^{-1}, and this initial decay is again followed by a slower rise. The amplitude of this rising transient relative to the B state maximum has increased from about 5% at 200 bar to 36% at 400 bar at $\lambda_{probe} = 298.5$ nm. It is observed that the relative amplitude has a maximum at this probe wavelength of 298.5 nm and decreases for both longer and shorter wavelengths. If LIF from the originally excited B state is subtracted (Figure 7a), we find that the rise time of this transient is significantly shorter (∼35 ps) than at 200 bar. An 800 ps transient taken at a probe wavelength of 277.5 nm shows that the recombination signal continues to increase slightly even after delay times of several hundred picoseconds. If the probe wavelength is changed to 321.5 nm, a strong decrease in the relative signal intensity at long times is noted. At the same time, the rise time decreases. At 332.3 nm, the signal intensity (now even smaller) is found to stay practically constant at delay times longer than 20 ps. If we probe at wavelengths longer than 340 nm, the B state decay is followed by a fast rise (approximately 6 ps) and a subsequent slower decay (∼35 ps). We note that even though the signal intensity is low and, consequently, the signal-to-noise ratio is relatively less, we discern fluorescence at delay times of more than 150 ps ($\lambda_{probe} = 355.0$ nm, 200 ps scan). The observed 35 ps decay is thus not a single exponential. At probe wavelengths longer than 358 nm, we detect only fluorescence from molecules on the B state. The decay rate of 0.45 ps^{-1} is identical to the one obtained at a probe wavelength of 310 nm, and the fluorescence intensity is equal to zero (within the signal-to-noise ratio) after 15 ps.

In the next figure (Figure 8a,b), we present transients at an argon pressure of 800 bar. It is evident from experiments with blue probe wavelengths (see e.g. $\lambda_{probe} = 299.5$ nm) that the relative amplitude of the recombination signal has increased by more than a factor of 2 compared to $p = 400$ bar. Its amplitude even exceeds the B state fluorescence amplitude, which now decays with a rate of 0.63 ps^{-1}. This increase in intensity of the recombination signal facilitates a more precise evaluation of the dynamics that follow the B state decay. We thus chose to perform more experiments at smaller probe wavelength intervals, especially in the red region above 345 nm. After subtracting the B state contribution to the total fluorescence signal, all transients for blue wavelengths between 275 and 310 nm appear similar, except for a change in relative amplitude, which reaches a maximum value of 1.22 at 299.5 nm. The rise for this transient is faster than at lower pressure and (nonsingle) exponential. The signal intensity at delay times between 200 and 800 ps shows no sign of a decrease and may even increase slightly.

When the wavelength was tuned to the red, a strong decrease in signal intensity at longer times was noticed. The shape of the transients after subtraction of the B state signal changes with wavelength in the following manner (in parentheses we include the relative amplitude at a delay time of 170 ps): 322 nm: faster rise time, no decay at long times ($a = 0.445$); 332 nm: quasi constant signal intensity for $t > 12$ ps ($a = 0.20$); note the peak in the signal at short delay times ($t \approx 15$ ps); 346.2 nm: fast rise followed by a slower decay to an approximately constant offset ($a = 0.13$); 355 nm: the rise and decay become more pronounced, and the offset decays to $a = 0.10$; 360.5 nm: decrease in the overall intensity of the recombination signal, at the same time the magnitude of the offset (or slow decay) at long times ($a = 0.06$) relative to the peak height of the fast rise and decay on the recombination signal decreases. A 25 ps transient (137 fs time delay between data points) allows for

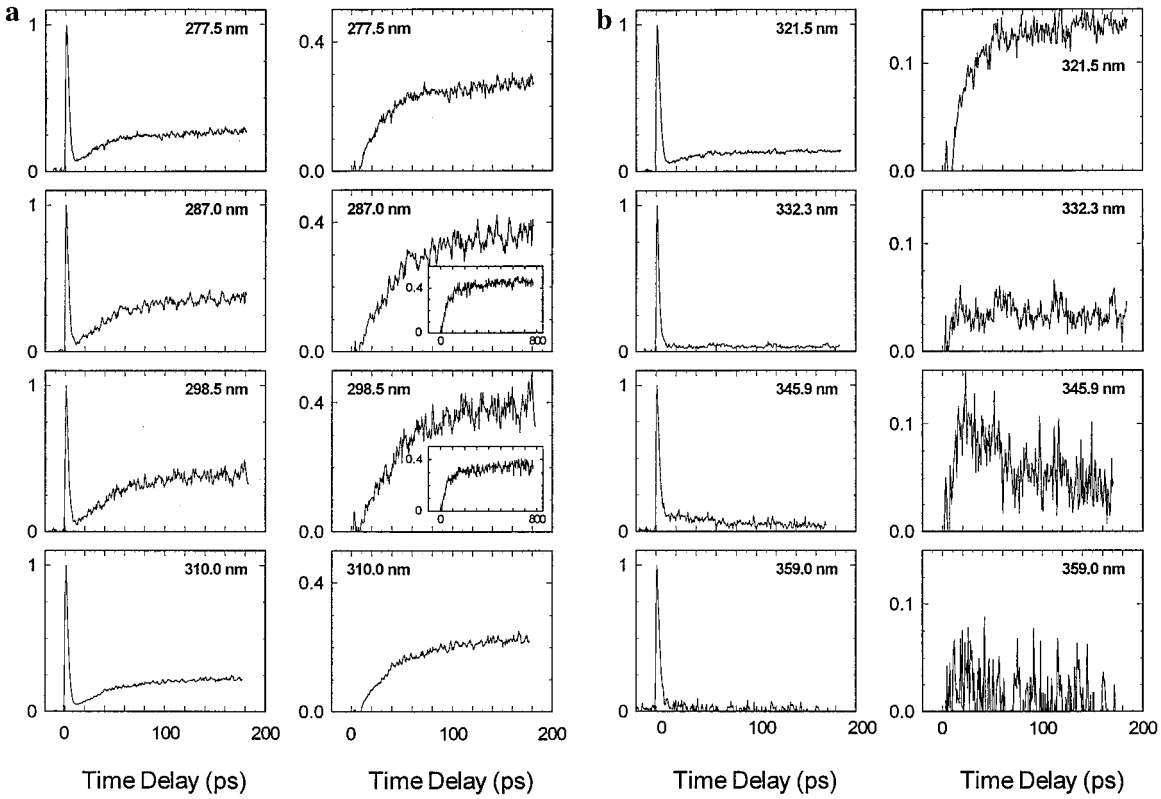

Figure 7. (a) Transients of iodine in compressed supercritical argon at a pressure of 400 bar on a time scale of 200 ps (0.67 ps/data point). The left column shows the original data while the right column shows the transients after subtraction of the B state fluorescence. Experiments have been recorded at 293 K using LIF detection at "magic" angle polarization between the pump (620 nm, 60 fs) and probe (variable wavelength between 277.5 and 310 nm, less than 150 fs) pulses. Signal amplitudes are normalized to the maximum in B state fluorescence intensity. The inserts show experiments performed under identical conditions on a time scale of 800 ps (2.67 ps/data point). Note the increase in fluorescence intensity at long delay times. (b) Transients of iodine in compressed supercritical argon at a pressure of 400 bar on a time scale of 200 ps (0.67 ps/data point) using probe wavelengths between 321.5 and 359.0 nm.

unequivocal separation of B state decay and recombination signal rise. At 363.3 nm the total recombination signal decreases, but fluorescence at long delay times of more than 100 ps is still observed. At probe wavelengths to the red of 363 nm, we are no longer able to detect signal from recombined iodine molecules. The transients reflect only the B state decay with a decay rate that is independent of the probe wavelength.

Increasing the pressure to 1200 bar (Figure 9) slightly changes the shape of the transients. At blue wavelengths a further increase in the recombination amplitude is observed, and the nonexponentiality of the rising transient becomes more pronounced. A fast rise (~13 ps) is followed by a steady slow increase in signal intensity over approximately 200 ps. The rise and decay on the recombination signal at red wavelengths become faster and more pronounced and can be more clearly separated from the slow decay or constant offset. An 800 ps transient taken at 355 nm displays a very slow decay at long times. The peak at early times represents the sum of B state decay and fast rise and decay of the recombination signal. Due to the long time interval between data points (2.7 ps), these processes can no longer be separated. It is also apparent that, compared to the 800 bar transients, the magnitude of the slow decay at long times relative to the peak height of the recombination signal decreases. At wavelength longer than 367 nm, we detect merely the B state decay with a probe-wavelength-independent rate of 0.80 ps^{-1}.

At a pressure of 1600 bar (Figure 10a−c), a series of pump−probe studies in the probe wavelength range from 275 to 391 nm was were performed. This procedure allows for a detailed comparison with the results obtained at an argon pressure of 800 bar. The transients in the blue region are now entirely dominated by the recombination signal. The fast decaying B state signal (lifetime $\tau = 1.05$ ps) appears only as a small peak at early times. The initial rise of the recombination signal is 9 ps, and the nonexponentiality of the entire rise is obvious. Transients at $\lambda_{probe} = 298.5$ and 307 nm indicate an increase in signal intensity up to delay times of 800 ps. At $\lambda_{probe} = 322$ nm, the amplitude of the recombination signal no longer exceeds the B state amplitude, and the rise time appears to be faster than at blue wavelengths. The transient at $\lambda_{probe} = 332$ nm shows a signal intensity that remains practically constant for time delays longer than 7 ps. If we tune further to the red, we observe the same features as at lower pressures: a fast rise followed by a slower decay and an offset (or rather very slow decay) at delay times longer than 25 ps. Higher resolution 25 ps transients reveal that the recombination signal amplitude reaches a maximum after ~7 ps and that this maximum shifts to shorter times as we increase the probe wavelengths (3 ps at 369.5 nm). We also find that the amplitude of this maximum relative to the signal intensity at long times (here 150 ps) increases steadily from 345 to 370 nm (0.48/0.28 at 345.2 nm vs 0.42/0.03 at 369.5 nm). The magnitude of this ratio in the extreme red (e.g., 14 at 369.5 nm) is larger than the same ratio at a pressure of 800 bar (e.g., 4.7 at 360.5 nm). This is equivalent to stating that the amplitude of the very slow decay is reduced at higher pressures. The 200 ps transient at $\lambda_{probe} = 369.5$ nm displays this slowly decaying transient. It should be noticed that the rate of the initial rise and decay on the recombination signal is faster at 1600 bar than at 800 bar. We emphasize that recombination fluorescence can be observed for wavelengths up to 372.5 nm, which should be compared to a "cutoff" wavelength of 363.3 nm at 800 bar.

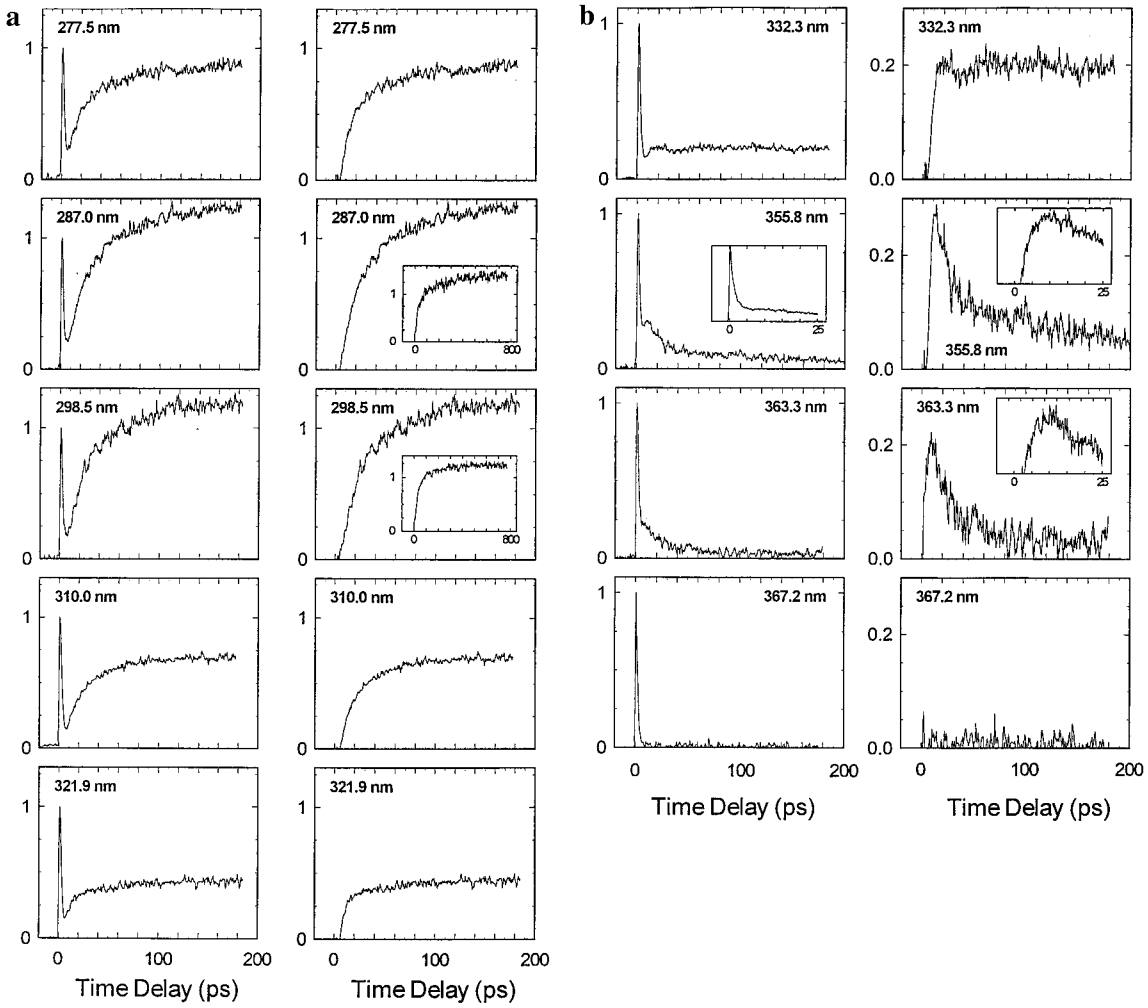

Figure 8. (a) Transients of iodine in compressed supercritical argon at a pressure of 800 bar on a time scale of 200 ps (0.67 ps/data point). The left column shows the original data while the right column shows the transients after subtraction of the B state fluorescence. Experiments have been recorded at 293 K using LIF detection at "magic" angle polarization between the pump (620 nm, 60 fs) and probe (variable wavelength between 277.5 and 321.9 nm, less than 150 fs) pulses. Signal amplitudes are normalized to the maximum in B state fluorescence intensity. The inserts show experiments performed under identical conditions on a time scale of 800 ps (2.67 ps/data point). (b) Transients of iodine in compressed supercritical argon at a pressure of 800 bar on a time scale of 200 ps (0.67 ps/data point) using probe wavelengths between 332.3 and 367.2 nm. The inserts show results obtained under identical conditions on a time scale of 25 ps (0.133 ps/data point).

Experiments have been performed at 2500 bar (Figure 11). For $\lambda_{probe} = 365.7$ nm (compare to the 25 ps transient at 1600 bar and 362.6 nm), the amplitude of the recombination signal is increased relative to a comparable transient at 1600 bar (see e.g. the 25 ps transient at 362.6 nm). At the same time an increase in the rise and decay rates after subtraction of the rapid B state decay ($\tau = 0.9$ ps) is noted. It is also interesting that the "cutoff" wavelength for detection of fluorescence from recombined iodine molecules is red-shifted to more than 377.5 nm.

V. Discussion

From the precise characterization of the B state dynamics in different solvents and at different pressures (preceding paper), we are able to subtract the B state contribution to the transients, leaving the temporal changes due to recombination dynamics. This subtraction was carried out as follows. A single-exponential decay $a \exp(-k_{pred}t)$, with k_{pred} for argon taken from Figure 12, was fitted to the B state fluorescence at early times and was then subtracted from the transient. The fluorescence in these so-obtained "recombination transients" reflects fluorescence from geminately recombined iodine molecules on either the A/A′ or the X state. Since a 310 nm pulse can only probe molecules in high vibrational levels on the X state (say $E_{vib} > 5000$ cm^{-1}) and vibrational relaxation through the upper part of the X state is known to be relatively fast in liquid xenon at room temperature,[68] we conclude that any signal that arises from X state molecules at these probe wavelengths must display a rise (which reflects the caging dynamics and the relaxation into the probe window) and a decay (reflecting vibrational relaxation out of the probe window). It is very reasonable to assume that the decay should not be longer than 100 ps at the highest pressures reached in our study and that the decay time should increase with decreasing pressure of the buffer gas. Such a fast rise and decay are not found for our transients at $\lambda_{probe} = 310$ nm. In fact, in the entire wavelength range from 277.5 to 310 nm, we observe that the signal intensity is monotonically rising for at least 800 ps. The very intense fluorescence at such long delay times cannot be attributed to X state molecules and is therefore due to molecules on the A or A′ state.

The A′ → D′ and A → β difference potentials (see Figure 4) indicate that absorption between 275 and 310 nm occurs at internuclear distances that are very close to the A and A′ state equilibrium distance. It is also known that the lifetime of the A and A′ state in liquid xenon is on the order of 10 ns (see Table 8 in ref 68), indicating that the fluorescence at these probe

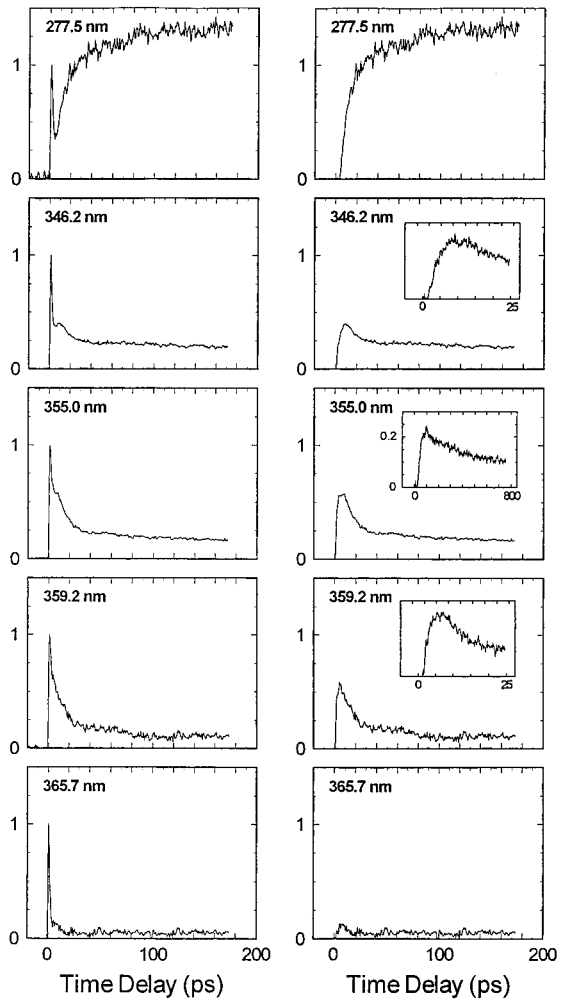

Figure 9. Transients of iodine in compressed supercritical argon at a pressure of 1200 bar on a time scale of 200 ps (0.67 ps/data point) using probe wavelengths between 277.5 and 365.7 nm. The left column shows the original data while the right column shows the transients after subtraction of the B state fluorescence. The inserts show results obtained under identical conditions on a time scale of 25 ps (0.133 ps/data point).

wavelengths arises from vibrationally relaxed molecules on the A or A′ state. In order to check the consistency of this assignment, we plot the intensities of A/A′ state fluorescence at delay times of 150 ps (on a 200 ps scan) relative to the maximum B state intensity at early times as a function of probe wavelength. Under the assumption that within this wavelength range the B state extinction coefficient does not strongly vary with wavelength, the deduced spectra should be similar to the gas-phase A′ → D′ spectra. This is indeed the case and is shown in Figure 13. As mentioned before, the D′ ← A′ and β ← A spectra are taken to be strongly overlapped, and the A and A′ state absorption is not separable in this analysis.

The fact that our experiments at wavelengths between 275 and 310 nm show no indication of the fast rise and decay that is expected to occur if fluorescence would arise from molecules recombining onto the X state has led us to conclude that the fluorescence induced by X state molecules is so weak that it does not significantly affect the overall shape of our transients. This does not mean that iodine molecules do not geminately recombine onto the X state, but rather that the extinction coefficient in high vibrational levels of the X state is much weaker than for molecules in the relaxed A or A′ states. It is known that the extinction coefficient for the D′ ← A′ transition from a relaxed A′ state distribution at 300 K is about 15 000 L mol^{-1} cm^{-1} at 295 nm[68] and that the extinction coefficient for ground-state iodine (which has a similar maximum value of 15 000 L mol^{-1} cm^{-1} at 184 nm at 300 K) drastically decreases with increasing vibrational level quantum number. Classically speaking, the molecules undergo a large-amplitude motion, and the probability for finding the molecule at the correct internuclear distance, where absorption can occur, decreases with increasing vibrational level quantum number. Accordingly, the transients in the probe range from 275 to 310 nm reflect the geminate recombination of iodine atoms on the A/A′ state surfaces and the subsequent vibrational relaxation within these states into the probe window, which is centered at the lowest vibrational levels of each state.

Another significant experimental finding is that the fluorescence from recombined iodine molecules can be observed up to a certain limiting wavelength in the red which we term the "cutoff wavelength". If we tune the probe laser wavelength further to the red, fluorescence originates solely from molecules on the originally excited B state. This cutoff wavelength depends on the argon pressure and changes from 363.3 nm at 800 bar to 372.5 nm at 1600 bar to more than 377 nm at 2500 bar. These values are in excellent agreement with the cutoff wavelengths estimated from pressure-dependent difference spectra (Figure 4), which are 364 nm at 800 bar and 370 nm at 1600 bar for the D′ ← A′ transition. D ← X transitions are energetically impossible at these wavelengths. The difference potentials also indicate that absorption at these wavelengths occurs only at internuclear distances that are much larger than the equilibrium A/A′ state distance. Hence, it is concluded that the fast rise and somewhat slower decay observed in the recombination transients at these wavelengths reflect the rapid geminate recombination of iodine molecules onto the A/A′ surfaces and vibrational relaxation through the probe window that is now centered at *high* vibrational levels. Tuning the probe laser to the blue will thus correspond to shifting the center of the probe window to lower vibrational levels.

In the intermediate probe wavelength range from 320 to 345 nm, where D ← X transitions from high vibrational X state levels are energetically allowed, we could only detect contributions to the transients that are consistent with A/A′ state dynamics. We thus take these transients also to reflect the dynamics of molecules trapped on these states with the fluorescence from X state molecules representing only a minor contribution. Transfer from the A/A′ states onto the X state occurs on a longer time scale (>5 ns) and cannot be detected in our 800 ps transients.

We now consider a simple kinetic model which takes into account the elementary steps of the reaction:

$$\mathrm{B} \xrightarrow{k_{\mathrm{pred}}} \mathrm{a} \xrightarrow{c(t),\, q_{\mathrm{A/A'}}} \mathrm{A}^* \xrightarrow{k_{\mathrm{VR}}} \mathrm{A} \quad \text{(nonadiabatic recombination)}$$

$$\mathrm{A}^{**} \xrightarrow{c(t),\, q_{\mathrm{A/A'}}} \mathrm{A}^* \xrightarrow{k_{\mathrm{VR}}} \mathrm{A} \quad \text{(adiabatic recombination)} \quad (2)$$

Molecules excited onto the B state predissociate onto the repulsive surface a (designating $a1_g(^3\Pi)$ or $a'0_g^+(^3\Sigma^-)$). These atoms then lose their excess kinetic energy and may form new molecules in the high vibrational levels (A*) on the A/A′ state potential. The quantum yield for this process is $q_{\mathrm{A/A'}}$. The time delay t between dissociation on the repulsive surface and the formation of a new iodine molecule is termed "recombination time". The function $c(t)$ therefore reflects the distribution in recombination times; i.e., it gives the probability that the formation of a new iodine molecule occurs at a time delay t after the dissociation of the original iodine molecule. The subsequent vibrational relaxation dynamics leads to low vibra-

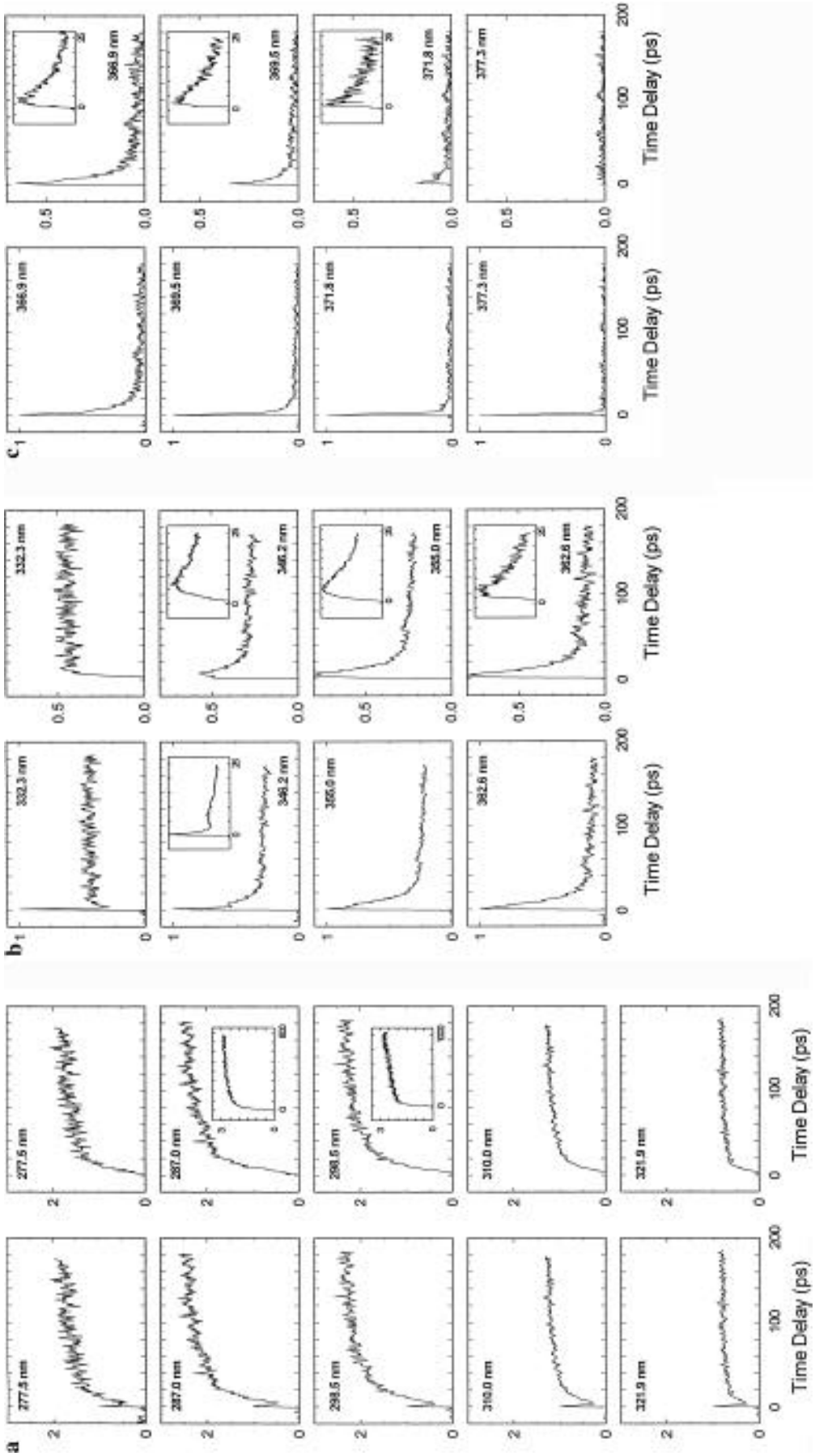

Figure 10. (a) Transients of iodine in compressed supercritical argon at a pressure of 1600 bar on a time scale of 200 ps (0.67 ps/data point) using probe wavelengths between 277.5 and 321.9 nm. The left column shows the original data while the right column shows the transients after subtraction of the B state fluorescence. The inserts show results obtained under identical conditions on a time scale of 800 ps (2.67 ps/data point). (b) Transients of iodine in compressed supercritical argon at a pressure of 1600 bar on a time scale of 200 ps (0.67 ps/data point) using probe wavelengths between 332.3 and 362.6 nm. The inserts show results obtained under identical conditions on a time scale of 25 ps (0.133 ps/data point). (c) Transients of iodine in compressed supercritical argon at a pressure of 1600 bar on a time scale of 200 ps (0.67 ps/data point) using probe wavelengths between 366.9 and 377.3 nm. The inserts show experiments performed under identical conditions on a time scale of 25 ps (0.133 ps/data point).

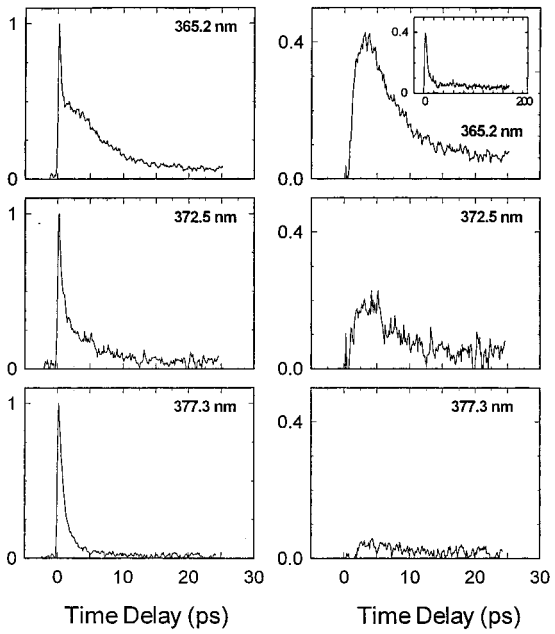

Figure 11. Transients of iodine in compressed supercritical argon at a pressure of 2500 bar on a time scale of 25 ps (0.133 ps/data point) using probe wavelengths between 365.2 and 377.3 nm. The left column shows the original data while the right column shows the transients after subtraction of the B state fluorescence. The insert shows results obtained under identical conditions on a time scale of 200 ps (0.67 ps/data point).

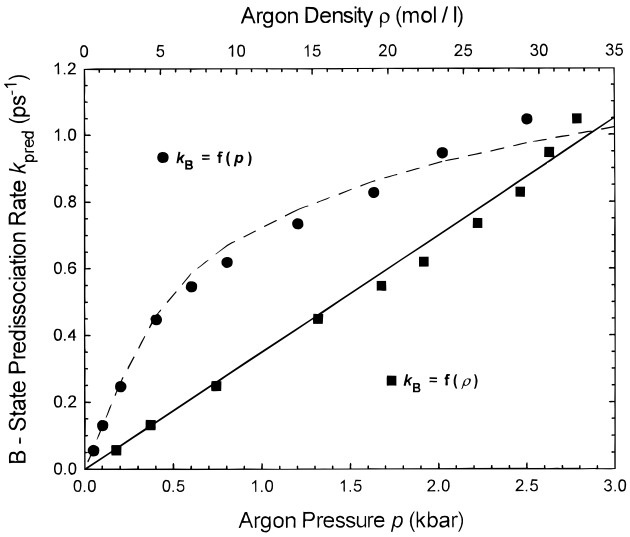

Figure 12. Rate for collision-induced predissociation k_{pred} of iodine in argon at an excitation wavelength of 620 nm as a function of argon pressure and argon density. The solid straight line shows the linear dependence between k_{pred} and argon density and indicates a quenching cross section $\sigma = 11.1$ Å^2 (see ref 1). The dashed linear line is the predicted change of predissociation rate with pressure, assuming $\sigma = 11.1$ Å^2 and a linear dependence between k_{pred} and ρ.

tional A/A′ state levels (A) and is described by the rate constant k_{VR}. We assume that the vibrational relaxation problem, which has in principle to be treated by a master equation approach for each vibrational level, can be reduced to a two-level relaxation between a "hot" level distribution A* and a "cold" level distribution A. It appears necessary to introduce this simplification because a more sophisticated formulation of the kinetic model (eq 2) would inevitably introduce additional free parameters. Finally, the molecules that are originally excited into the repulsive branch of the A state (A**) undergo similar caging and vibrational relaxation dynamics as those on the repulsive

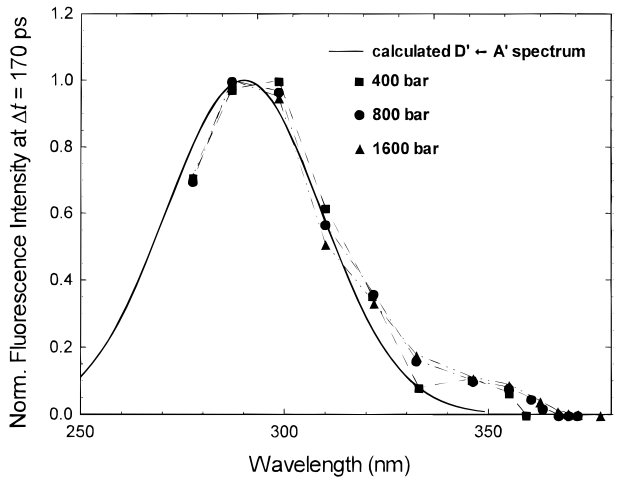

Figure 13. Comparison between calculated D′ ← A′ absorption spectrum[103] for gas-phase iodine at $T = 300$ K and experimentally observed normalized relative fluorescence intensities a at a delay time $\Delta t = 170$ ps. Relative fluorescence intensities a ($\Delta t = 170$ ps, λ_{probe}) are obtained by normalizing the intensity in each transient at $\Delta t = 170$ ps on a 200 ps transient onto the maximum B state fluorescence intensities at delay times shorter than 1 ps. In order to compare intensities at different pressures, the so obtained relative fluorescence intensities at a given pressure are then normalized.

$a1_g(^3\Pi)$ or $a'0_g^+(^3\Sigma^-)$ surfaces, except for the *adiabatic* nature of this motion from $t = 0$ until completion.

The total fluorescence signal $s(t)$ in our transients is then given as $s(t) = a_B[B(t)] + a_{A^*}[A^*(t)] + a_A[A(t)]$, where the amplitudes a_B, a_{A^*}, and a_A reflect the wavelength-dependent absorption cross sections in the respective states. As discussed before, the B state contribution can be accurately subtracted, and this leaves the "recombination signal" $r(t) = a_{A^*}[A^*(t)] + a_A[A(t)]$. The following system of differential equations can now be written explicitly:

$$[\dot{B}(t)] = -k_{pred}[B(t)], \quad [B(t{=}0)] = p_B N_0, \quad [B(t{\le}0)] = 0$$

$$[\dot{a}(t)] = k_{pred}[B(t)] + \int_{-\infty}^{t}[\dot{B}(t')]q_{A/A'}c(t-t')\,dt', \qquad [a(t{\le}0)] = 0$$

$$[\dot{A}^{**}(t)] = -\delta(t)[A^{**}(t)], \quad [A^{**}(t{=}0)] = p_A N_0, \qquad [A^{**}(t{\le}0)] = 0$$

$$[\dot{A}^*(t)] = -\int_{-\infty}^{t}([\dot{B}(t')] + [\dot{A}^{**}(t')])q_{A/A'}c(t-t')\,dt' - k_{VR}[A^*(t)], \quad [A^*(t{\le}0)] = 0$$

$$[\dot{A}(t)] = k_{VR}[A^*(t)], \quad [A(t{\le}0)] = 0 \qquad (3)$$

In eq 3, p_B denotes the probability for exciting the B state (62% at $\lambda_{pump} = 620$ nm) and p_A for exciting the A state (34% at $\lambda_{pump} = 620$ nm). In order to solve this system of differential equations, we need to assume specific model functions for the distribution of recombination times $c(t)$. First, we will assume that caging is entirely dominated by extremely rapid primary recombination (as was indicated by experiments in liquid solvents[69]). This is equivalent to a case where recombination can only occur as long as molecules are imprisoned inside the *solvent cage* as clearly evident in studies of iodine in argon clusters where coherent solvent caging was observed on the subpicosecond time scale.

If molecules break out of the cage, the probability for recombination is thought to be negligible (**no** diffusive or secondary recombination). It is then reasonable to assume a

very narrow distribution of caging times, and we will approximate this distribution by a function of the form

$$c(t) = \begin{cases} 0, & t < \Delta t \\ k_{\text{cage}} \exp(-k_{\text{cage}}(t-\Delta t)), & t \geq \Delta t \end{cases} \quad (4)$$

We note that this function differs significantly from analytical distribution functions obtained from diffusion-based models.[5,6] Such a choice, however, has the advantage that it allows for an analytical solution of the differential equations (eq 3). The total fluorescence signal $s(t)$ is then given as a sum of three exponentials: $s(t) = a_1 \exp(-k_{\text{pred}}t) + a_2 \exp(-k_{\text{cage}}t) + a_3 \exp(-k_{\text{VR}}t)$. At pressures of 800 bar and above, all three rate constants have to be faster than $(20\ \text{ps})^{-1}$ in order to give agreement with the experimentally observed short-time dynamics. There is, however, no possible choice for these three rate constants that can reproduce the **slow** decays observed at red wavelengths or the **slow** signal increases (over several hundred picoseconds) at blue wavelengths (275−310 nm).

Such a slow fluorescence decay is observed even at the most red wavelengths at a pressure of 1600 bar (see for example the transients at $\lambda_{\text{probe}} = 363$, 367, or 372 nm). Since these wavelengths correspond to probing A/A′ state iodine at large internuclear distances (or in high vibrational levels near the dissociation threshold), these slow decays cannot be attributed to incomplete vibrational relaxation. Thus, our experiments strongly indicate that a very narrow distribution of caging times as assumed in eq 4 does not correctly describe the recombination dynamics in high-pressure rare-gas solvents. A correct distribution function has to account for recombination acts occurring on a time scale of hundreds of picoseconds. These correspond to iodine atoms that break out of the solvent cage and recombine diffusively ("secondary recombination"). We incorporate these processes in our model by assuming a biexponential distribution function for caging times:

$$c(t) = \begin{cases} 0, & t < \Delta t \\ p_{\text{fast}} k_{\text{cage}}^{\text{fast}} \exp(-k_{\text{cage}}^{\text{fast}}(t-\Delta t)) + (1-p_{\text{fast}}) k_{\text{cage}}^{\text{slow}} \exp(-k_{\text{cage}}^{\text{slow}}(t-\Delta t)), & t \geq \Delta t \end{cases} \quad (5)$$

Here p_{fast} denotes the probability for fast ("primary") vs slow ("secondary") recombination, and $k_{\text{cage}}^{\text{fast}}$ and $k_{\text{cage}}^{\text{slow}}$ are the rates for the respective processes. The total fluorescence signal is then given as a sum of four exponentials:

$$s(t) = a_1 \exp(-k_{\text{pred}}t) + a_2 \exp(-k_{\text{cage}}^{\text{fast}}t) + a_3 \exp(-k_{\text{cage}}^{\text{slow}}t) + a_4 \exp(-k_{\text{VR}}t) \quad (6)$$

Three of the rate constants are free parameters in the simulations: $k_{\text{cage}}^{\text{fast}}$, $k_{\text{cage}}^{\text{slow}}$ (characterizing $c(t)$), and k_{VR}, representing the A/A′ state vibrational relaxation rate. Furthermore, the amplitudes a_1 to a_4 are functions of Δt, k_{pred}, $k_{\text{cage}}^{\text{fast}}$, $k_{\text{cage}}^{\text{slow}}$, k_{VR}, p_{fast}, a_{A^*}, and a_{A}. Here, Δt, p_{fast}, a_{A^*}, and a_{A} are free fitting parameters. This leaves a total of seven free parameters. Four of these parameters Δt, $k_{\text{cage}}^{\text{fast}}$, $k_{\text{cage}}^{\text{slow}}$, and p_{fast} are dependent on pressure but should be independent of the probe wavelength at a given pressure. The vibrational relaxation rate should in principle decrease as we shift the probe window from high to low vibrational levels (from red to blue wavelengths). Such a trend has indeed been observed at $p = 1600$ bar; however, the change in k_{VR} was only slightly larger than the error in k_{VR} $(0.11 \pm 0.04\ \text{ps}^{-1})$, so that k_{VR} was assumed to be independent of wavelength. We fitted five of the seven free parameters globally to all transients at a given pressure. This left only two independent parameters at each wavelength: a_{A^*} and a_{A}. Their absolute magnitude fits the overall amplitude of the transient, and their ratio $a_{\text{A}}/a_{\text{A}^*}$ reflects the shift in the probe window from low to high vibrational levels. As expected, we found in the simulation that this ratio changes monotonically from values close to zero at red wavelengths to values much larger than unity for $\lambda_{\text{probe}} = 275-310$ nm.

Obtaining a consistent set of parameters required extensive analysis of the data set at each pressure. Generally, we proceeded as follows. We determined $k_{\text{cage}}^{\text{fast}}$ and k_{VR} from experiments at red wavelengths and then checked the consistency of these values at blue wavelengths from which we also obtained p_{fast}. If we noticed inconsistencies, we repeated the analysis with an improved set of parameters until we obtained a self-consistent parameter set that reproduced best the entire data set at a given pressure. The values for a_{A^*} and a_{A} were optimized at each wavelength without restrictions. It turned out to be difficult to extract a precise value for $k_{\text{cage}}^{\text{slow}}$. In most transients $k_{\text{cage}}^{\text{slow}}$ could be varied over a relatively wide range without significantly affecting the quality of the fits, especially at lower pressures. We thus used the optimum value at 1600 bar ($k_{\text{cage}}^{\text{slow}} = 0.005\ \text{ps}^{-1}$) at all pressures, even though we noticed a slight tendency for $k_{\text{cage}}^{\text{slow}}$ to decrease at lower pressures. The optimal parameters obtained from the data analysis are summarized in Table 1.

Comparisons between the actual data and simulations using the parameters in Table 1 are shown in Figure 14. We notice that the general agreement is good. One observes slight discrepancies between experiment and simulation at intermediate probe wavelengths from 330 to 345 nm. This is not surprising, as at these wavelengths iodine is probed in vibrationally relaxed and intermediate vibrational levels on the A/A′ state with similar weight. In this case the assumption of a simple two-level distribution A* and A with a single-exponential relaxation rate is expected to be too gross a simplification, and it should be necessary to consider the dependence of the vibrational relaxation rate on the vibrational energy. In fact, the introduction of an intermediate level A^+ between A* and A and of a second (slower) vibrational relaxation rate k'_{VR} from A^+ to A removes the observed discrepancies.

The comparison between experimental results and theoretical predictions of the model strongly supports our previous conclusion that the experimental transients reflect the geminate recombination of iodine onto the A/A′ state potentials and the subsequent vibrational relaxation within these states. Tuning the probe laser from the blue to the red corresponds to shifting the probe window from internuclear distances close to the A/A′ state equilibrium distance (low vibrational levels) to larger distances or higher vibrational levels. The accumulation of a thermally equilibrated population centered at $v' = 0$ is probed from 275 to 310 nm, while the signal peak at red wavelengths reflects the buildup and decay of population at internuclear distances larger than the A/A′ state equilibrium distance. At intermediate wavelengths, a superposition of vibrationally relaxed and vibrationally excited molecules is probed, which explains the offset observed after the initial signal peak. The total rate for vibrational relaxation within the A/A′ states decreases with decreasing pressure from $0.20 \pm 0.12\ \text{ps}^{-1}$ at 2500 bar, $0.11 \pm 0.04\ \text{ps}^{-1}$ at 1600 bar, to $0.029 \pm 0.008\ \text{ps}^{-1}$ at 400 bar, as one would expect based on a simplified binary collision model (see Figure 15).

Our data also provide information about the distribution of recombination times $c(t)$ and how this distribution is affected by softening the solvent cage when decreasing the pressure. Pressure-dependent distribution functions obtained from the

TABLE 1: Experimental Results for the Dissociation and Geminate Recombination of Iodine in Compressed Argon at 293 K as a Function of Solvent Pressure[a]

press. (bar)	k_{pred} (ps^{-1})	k_{cage}^{fast} (ps^{-1})	k_{cage}^{slow} (ps^{-1})	k_{VR} (ps^{-1})	Δt (ps)	p_{fast}
200	0.25		0.0033	0.017		
400	0.45	0.17	0.005	0.029	7	0.78
800	0.63	0.33	0.005	0.050	3	0.73
1200	0.80	0.67	0.005	0.077	1.4	0.73
1600	0.95	1.25	0.005	0.120	0.3	0.70
2500	1.11	1.67	0.005	0.200	0.5	

[a] Results are obtained by globally fitting the experimental transients $s(t)$ at all probe wavelengths to a sum of four exponentials: $s(t) = a_1 \exp(-k_{pred}t) + a_2 \exp(-k_{cage}^{fast}t) + a_3 \exp(-k_{cage}^{slow}t) + a_4 \exp(-k_{VR}t)$, as indicated by the kinetic model (eq 2) presented in the text, if a biexponential distribution for the caging times (eq 6) is assumed. k_{pred} denotes the B state predissociation rate, p_{fast} is the probability for fast ("primary") vs slow ("secondary") recombination, and k_{cage}^{fast} and k_{cage}^{slow} are the rates for the respective processes. k_{VR} corresponds to the rate for vibrational relaxation within the A/A′ states.

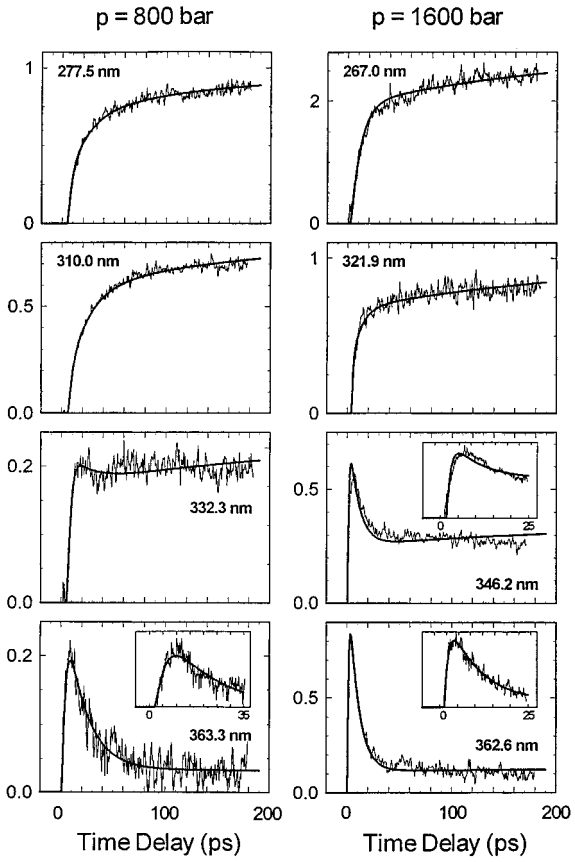

Figure 14. Comparison between experimentally observed pump−probe transients and simulatiopns using the kinetic model (eq 2). Comparisons are shown for argon pressures of 800 and 1600 bar. Identical parameters for the B state predissociation rate k_{pred}, the distribution of recombination times $c(t)$, and the A/A′ state vibrational relaxation rate k_{VR} have been used in all simulations at a given pressure. Values of these parameters are given in Table 1.

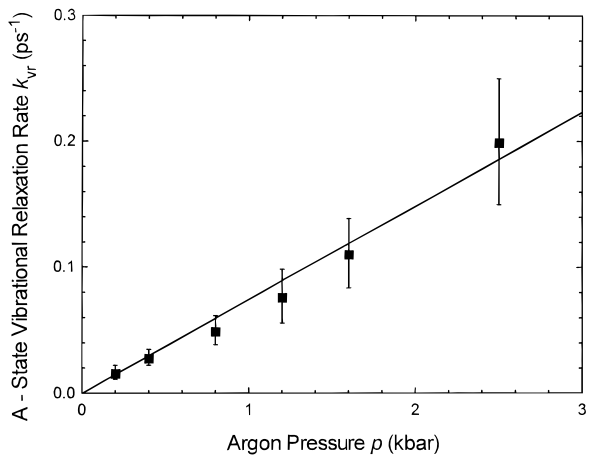

Figure 15. A/A′ state vibrational relaxation rates k_{VR} as a function of argon pressure, as obtained by simulation of the femtosecond transients using the kinetic model (eq 2).

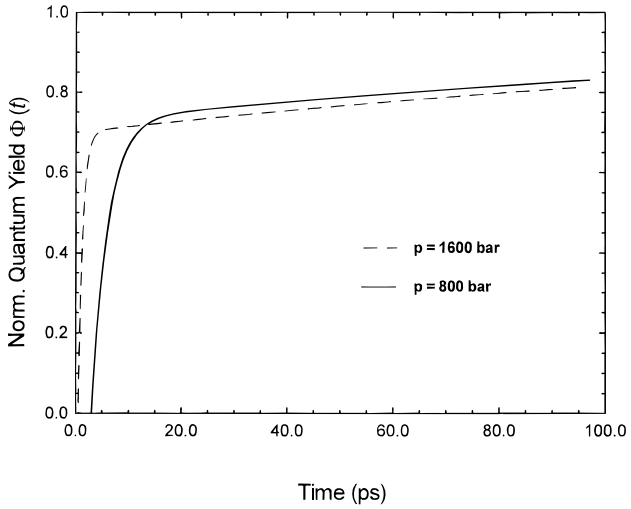

Figure 16. Time-dependent geminate recombination probability $\phi(t)$ of iodine in supercritical argon at pressures of 800 and 1600 bar, as obtained by kinetic analysis of the femtosecond transients using (eq 2). $\Phi(t)$ is calculated by integration of the biexponential distribution of recombination times $c(t)$ (eq 5), $\Phi(t) = \int_0^t c(t')\,dt'$. Pressure-dependent values of k_{cage}^{fast}, k_{cage}^{slow}, and p_{fast} are taken from Table 1.

simulations are shown in Figure 16. At high pressures (p = 1600 and 2500 bar), most iodine atoms can be observed to recombine extremely rapidly ($k_{cage}^{fast} > 1$ ps^{-1}). These atoms immediately lose their excess kinetic energy to the very rigid first solvent shell that is closely packed around the iodine atoms, and a fraction p_{rec} of them then form a new iodine molecule within the solvent cage. (This corresponds to what is loosely called "primary recombination".) There is, however, a finite probability ($1 - p_{rec}$) for the atoms to break out of the solvent cage. Once outside the cage, these molecules will start a diffusive motion through the solvent and might eventually diffuse back into the solvent cage. Those which entered the cage will then have to decide again whether to react (p_{rec}) or to leave the cage again. This *diffusive* recombination is observed in our experiments to occur on a much longer time scale ($k_{cage}^{slow} = 0.005$ ps^{-1}) and corresponds to what has been termed *"diffusive secondary recombination"*.

Decreasing the pressure softens the solvent cage (p = 1200 bar) and thus increases the probability ($1 - p_{rec}$) for breaking out of the cage. At the same time, the mobility of iodine atoms increases (the diffusion coefficient is inversely proportional to the density), and the overall quantum yield for geminate recombination decreases. The softer cage structure will not only

affect the probability of the different processes. but also slow down the rate for loss of kinetic energy and subsequent primary recombination. At pressures below 1000 bar, the cage structure becomes so loose that primary and fast diffusive recombination acts intermingle and that the clear distinction between both processes, which is evident at the highest pressures in our study, gradually vanishes. This is reflected in the finding that the distinct biexponentiality in the recombination signal rise for blue probe wavelengths at $p = 1600$ bar becomes less obvious as we decrease the pressure.

At the lowest pressures of this study, $p = 100$ and 200 bar, it is no longer appropriate to define a specific solvent cage. The iodine atoms can now reach large internuclear separations before they lose their excess kinetic energy. Due to the high mobility of the iodine atoms, it becomes unlikely that an iodine atom finds its way back to its original partner atom. At pressures below 200 bar of argon, the recombination of dissociated iodine atoms is entirely dominated by diffusive nongeminate recombination.

It is instructive to consider the above picture in relation to a theoretical, diffusion-based model for the atomic recombination of iodine in dense media that has recently been proposed by Otto, Schroeder, and Troe.[16] As we discussed in the preceding paper,[1] this model is able to accurately predict the solvent effect on the time-integrated quantum yield for geminate atomic recombination of iodine in compressed supercritical solvents. In this model the recombination dynamics is split into two steps: initial separation of the two iodine atoms under the influence of the repulsive potential and subsequent diffusive motion of the separated iodine atoms.

In the first step, the iodine atoms separate on the repulsive $a1_g(^3\Pi)$ or $a'0_g^+(^3\Sigma^-)$ potential and lose their excess kinetic energy to the solvent. It is assumed that after energy equilibration all atoms are located at a specific internuclear distance r_0. This distance can be calculated analytically if the repulsive potential is approximated by a truncated harmonic potential and if the atoms are assumed to experience a macroscopic friction force of the Stokes type. In the next step of the recombination process, the atoms start a diffusive motion through the solvent. Each time, their internuclear distance reaches a certain contact distance R_c (which can be approximated using Lennard-Jones diameters of iodine and argon atoms); the atoms can decide whether to recombine or to diffuse apart. The probability for recombination is given by the ratio of the rate for collisional stabilization of the encounter pair versus the rate for diffusional separation. The fraction $\Phi(t)$ of molecules that have recombined after a time delay t can then be evaluated analytically by solving the diffusion equation using the partially reflecting boundary condition suggested by Collins and Kimball.[70] We refer to the paper by Otto, Schroeder, and Troe and ref 1 for a more detailed discussion of the model and a derivation of $\Phi(t)$.

The evaluation of $\Phi(t)$ for iodine in argon at a pressure of 1600 bar shows a similar biphasic recombination dynamics as observed in our experiments. (See Figure 17, where we normalize $\Phi(t)$ to $\Phi(\infty)$, for better comparison between data at different pressures.) In this model, the initial separation of the iodine atoms r_0 at this pressure is only slightly larger than the encounter radius R_c. Thus, a large fraction of the molecules can react immediately after the initial separation. A smaller fraction, however, can reach larger internuclear distances and than diffuse back to the original partner atom. As the pressure is lowered, the distinction between both recombination mechanisms is less obvious. This reflects the increase in the diffusion coefficient and thus the higher mobility of the iodine atoms. Even though this model cannot predict the coherent, primary

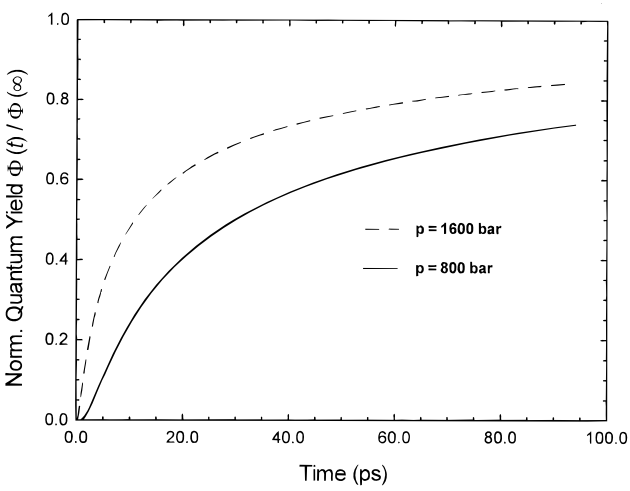

Figure 17. Time-dependent recombination probability $\Phi(t)/\Phi(\infty)$ for iodine in supercritical argon at 800 and 1600 bar as obtained from the diffusion-based model by Otto, Schroeder, and Troe.[16] $\Phi(t)$ was used as given in eq 4.16 in ref 16. Note the biphasic recombination dynamics at high pressures.

ultrafast in-cage recombination dynamics, it identifies the subsequent mechanism that is dominating the recombination.

The overall picture now develops from the above dynamical studies of the real time motion and of the yield: An initial separation and loss of kinetic energy, an extremely rapid recombination of atoms that are imprisoned inside the *solvent cage*, as well as a diffusive geminate recombination of atoms that are able to break out of this cage. The process of in-cage recombination in dense solvents must relate to the case of iodine synthesized in a cluster solvent cage, the limiting case of "frozen" solvent cages.

Liu *et al.*[71−74] studied the ultrafast cage-induced recombination of iodine in large Ar_n clusters. They observed the first coherent, adiabatic recombination in ∼700 fs following the caging dynamics. The results clearly indicate the dynamics of the recombination in the solvent cage and elucidate the effect of the solvent cage structure (rigidity, temperature, etc.) on the time scale of recombination. At the probe wavelength of 310 nm, the recombination dynamics is followed by a slower (∼30 ps) buildup, which resembles the dynamics observed in high pressure. Based on the probe-tuning analysis given here, the signal at long delay times reflects the accumulation of iodine molecules in low vibrational A/A′ state levels (not the X state). A recent probe-wavelength-dependent study by Liu et al. supports this analysis.[73] From the cluster studies and molecular dynamics simulations two concepts emerged. First is the importance of the time scale for bond breakage on the dynamics of the bond remaking; the longer the time scale for the former, the less coherent and prompt the latter. Second is the effect of the solvent motion on the persistence of coherence; the more rigid the structure, the more persistent the coherent motion. Clearly, the solvent barrier at short times represent a highly nonequilibrium state of the solvent; at equilibrium and with solvent motion and reorganization the barrier is relatively much smaller in height. This picture was supported by molecular dynamics simulations.[72−74]

Recently, Apkarian and co-workers studied the same system in matrices at low temperatures, and Martens' group provided the microscopic picture using molecular dynamics.[75−77] They showed the coherent recombination dynamics in argon matrices when iodine was excited above the A state dissociation limit. As noted in ref 71, in such cold matrices, iodine molecules are surrounded by a very rigid solvent structure which also prevents dissociating iodine atoms from breaking through the solvent

cage. In the matrix, the cage-induced recombination occurs on the A or A′ state within approximately 1 ps, similar to the cluster. A variety of UV probe wavelengths ranging from 319 to 364 nm have been used to interrogate the dynamics of molecules in different vibrational levels on the A and A′ states, and the authors concluded that no evidence for fluorescence from ground-state iodine molecules was detected. In our earlier 310 nm probing,[17−19] we could not separate the contribution of A/A′ or X state recombination, and we discussed X state caging, but as shown here, through probe tuning, the A/A′ state recombination is probed, consistent with the matrix work.[75−77] For clusters, with similar probing the A state recombination was similarly established.[73,74] Finally, through variation of the probe wavelength the vibrational relaxation dynamics within the A/A′ state was also studied and found to occur on a somewhat longer time scale than in room-temperature argon at high pressures (p = 1600 bar, see Figure 15 here and the results in ref 1).

In liquids, experiments in which the dynamics of iodine is interrogated by UV laser pulses are not as common as at other, longer wavelengths. In an early paper,[78] Harris et al. reported on the UV transient absorption of iodine in CCl_4 and hexane after excitation with 590 nm pulses. The probe wavelength dependence of the reported transients strongly resembles the transients that were reported here in argon at a pressure of 1600 bar. It is thus likely that the UV absorption in these experiments reflects not only the B state predissociation, which is too fast to be resolved, but also the fast geminate recombination and the subsequent vibrational relaxation within the A/A′ state. If analyzed in terms of the kinetic model presented above, these experiments would suggest an A/A′ state vibrational relaxation rate of $(5-10\ \text{ps})^{-1}$, which is comparable to the rate observed in argon at the highest pressures. This model is also consistent with the recent experiment in liquid CCl_4.[79]

VI. Summary and Conclusion

In this contribution we report the femtosecond to subnanosecond dissociation and recombination dynamics of iodine in highly compressed supercritical argon: at pressures between 0 and 2500 bar. Variation of the pressure made it possible to study the elementary reaction dynamics at densities spanning the gas-to-liquid transition region. As detailed in the preceding paper, in argon the wave packet motion on the iodine B state surface maintains its coherence for several picoseconds at pressures as high as 800 bar. The collision-induced B state predissociation rate increases linearly with the density of the solvent and reaches 0.9 ps at the highest density (33 mol L^{-1} or 20 atoms/nm^3) at 2500 bar. The change in predissociation rate with density indicates a pressure-independent reaction probability per collision and reflects the importance of the short-range binary collision forces in determining the dynamics. This makes the rates insensitive to details of the attractive forces which could give rise to clustering of Ar solvent. Their influence will be more pronounced in the solvent-induced fluorescent shift and wave packet mean frequency.

Of particular focus here was the nature of the recombination dynamics as the solvent structure changes its characteristics at different densities. We interrogated the geminate recombination dynamics of the dissociating iodine atoms with femtosecond resolution and along the reaction coordinate with probe tunability from 275 to 400 nm. The transients indicate that the fluorescence induced by the UV probe lasers in this wavelength region originates primarily from iodine molecules that recombine onto the A or A′ state potentials. With this tunability we could probe the initial geminate recombination dynamics and the vibrational energy relaxation of the newly-formed iodine molecules within these states. This analysis is consistent with known gas-phase potentials and with the experimentally observed solvent-induced fluorescence shifts. It is supported by the relatively small changes of the potential found from studies of the wave packet coherent motion at high densities (preceding paper).

Our results indicate that in supercritical rare gas solvents at high pressures two geminate recombination processes can be distinguished. It is essential that a correct physical interpretation of the caging dynamics predicts this *distribution* of recombination times. A large fraction of the dissociated iodine atoms distributes its excess energy to the surrounding solvent atoms and undergoes ultrafast recombination within the first solvent shell. The remaining atoms leave that cage and recombine diffusively on a much longer time scale. By decreasing the solvent pressure, we can increase the probability for breaking out of the solvent cage and thereby affect not only the overall quantum yield for geminate recombination but also the distribution function of recombination times. These changes in the elementary reaction dynamics were observed with fs resolution and compared with dynamical models which incorporate the key processes of solute−solvent interactions.

Acknowledgment. This work was supported by the National Science Foundation. Ch.L. and A.M. gratefully acknowledge a postdoctoral fellowship by the Deutsche Forschungsgemeinschaft.

References and Notes

(1) Lienau, Ch.; Zewail, A. H. *J. Phys. Chem.* **1996**, *100*, 18629.
(2) Franck, J.; Rabinowitch, E. *Trans. Faraday Soc.* **1934,** *30*, 120.
(3) Rabinowitch, E.; Wood, W. C. *Trans. Faraday Soc.* **1936,** *32*, 547, 1381.
(4) Zimmerman, J.; Noyes, R. M. *J. Chem. Phys.* **1950,** *18*, 658.
(5) Booth, D.; Noyes, R. M. *J. Am. Chem. Soc.* **1960,** *82*, 1868.
(6) Meadows, L. F.; Noyes, R. M. *J. Am. Chem. Soc.* **1960,** *82*, 1872.
(7) Bunker, D. L.; Davidson, N. *J. Am. Chem. Soc.* **1958**, *80*, 5090.
(8) Porter, G.; Smith, J. A. *Proc. R. Soc. London, Ser. A* **1961**, *261*, 28.
(9) Schroeder, J.; Troe, J. *Annu. Rev. Phys. Chem.* **1987,** *38*, 163.
(10) Troe, J. *J. Phys. Chem.* **1986**, *90*, 357.
(11) Hippler, H.; Schubert, V.; Troe, J. *J. Chem. Phys.* **1984**, *81*, 3931.
(12) Luther, K.; Troe, J. *Chem. Phys. Lett.* **1974**, *24*, 85.
(13) Hippler, H.; Luther, K.; Troe, J. *Ber. Bunsen-Ges. Phys. Chem.* **1973**, *77*, 1104.
(14) Dutoit, J. C.; Zellweger, J. M.; van den Bergh, H. *J. Chem. Phys.* **1983**, *78*, 1825.
(15) Zellweger, J. M.; van den Bergh, H. *J. Chem. Phys.* **1980**, *72*, 5405.
(16) Otto, B.; Schroeder, J.; Troe, J. *J. Chem. Phys.* **1984**, *81*, 202.
(17) Lienau, Ch.; Williamson, J. C.; Zewail, A. H. *Chem. Phys. Lett.* **1993**, *213***,** 289.
(18) Lienau, Ch.; Zewail, A. H. *Chem. Phys. Lett.* **1994**, *218***,** 224.
(19) Lienau, Ch.; Zewail, A. H. *J. Chim. Phys. Phys.-Chim. Biol.* **1995**, *92***,** 566.
(20) The electronic states are designated by the letters X, A, A′, etc., followed by a symmetry label A_b^c, which is appropriate for Hund's case (c) (strong interaction between the electronic spin and orbital angular momentum). A gives the quantum number Ω or the absolute value of the projection of the **total** electronic angular momentum on the internuclear axis. The subscript b denotes the symmetry "g" or "u" under inversion in a fixed molecular frame. In the case of states with Ω = 0, an additional superscript "+" or "−" decribes the behavior of the wave function under reflection in a plane through both nuclei. The electric dipole selection rules for electronic transitions are $\Delta\Omega = 0, \pm 1$ and g ↮ u, with the additional selection rule that $0^+ \nleftrightarrow 0^-$ are forbidden. Hund's case (a) labels (superscript $2S + 1$ for the total electronic spin and capital letters Σ, Π, Δ, for the component of the electronic orbital angular momentum along the internuclear axis) which are relevant for discussion of intensities follow the case (c) labels in parentheses. The additional case (a) selection rules are $\Delta\Lambda = 0, \pm 1$, and $\Delta S = 0$.
(21) Gerstenkorn, S.; Luc, P. *J. Phys. (Paris)* **1985**, *46*, 867.
(22) Bowman, R. M.; Dantus, M.; Zewail, A. H. *Chem. Phys. Lett.* **1989**, *161*, 297.
(23) Dantus, M.; Bowman, R. M.; Zewail, A. H. *Nature* **1990**, *343*, 737.
(24) Dunham, J. L. *Phys. Rev.* **1932**, *41*, 721.
(25) Rydberg, R. *Z. Phys* **1931**, *73*, 376; **1933**, *80*, 514.
(26) Klein, O. *Z. Phys.* **1932**, *76*, 226.

(27) Rees, A. L. G. *PWC Phys. Soc.* **1947**, *59*, 948.
(28) Tellinghuisen, J. *J. Comput. Phys. Commun.* **1974**, *6*, 221.
(29) Gruebele, M.; Zewail, A. H. *J. Chem. Phys.* **1993**, *98*, 894.
(30) Gruebele, M. *Mol. Phys.* **1990**, *69*, 475.
(31) Zheng, X.; Fei, S.; Heaven, M. C.; Tellinghuisen, J. *J. Chem. Phys.* **1992**, *96*, 4877.
(32) Visnawathan, K. S.; Sur, A.; Tellinghuisen, J. *J. Mol. Spectrosc.* **1981**, *86*, 393.
(33) Tellinghuisen, J. *J. Chem. Phys.* **1985**, *82*, 4012.
(34) Churassy, S.; Martin, F.; Bacis, R.; Vergès, J.; Field, R. W. *J. Chem. Phys.* **1981**, *75*, 4863.
(35) Martin, F.; Churassy, S.; Bacis, R.; Vergès, J.; Field, R. W. *J. Chem. Phys.* **1983**, *79*, 3725.
(36) Lawley, K. P.; Donovan, R. J. *J. Chem. Soc., Faraday Trans.* **1993**, *89*, 1885.
(37) Jewsbury, P. J.; Ridley, T.; Lawley, K. P.; Donovan, R. J. *J. Mol. Spectrosc.* **1993**, *157*, 33.
(38) Lawley, K. P.; Jewsbury, P. J.; Ridley, T.; Langridge-Smith, P.; Donovan, R. *J. Mol. Phys.* **1992**, *75*, 811.
(39) Zheng, X.; Fei, S.; Heaven, M. C. *J. Mol. Spectrosc.* **1991**, *149*, 399.
(40) Bartels, M.; Donovan, R. J.; Holmes, A. J.; Langridge-Smith, P.; MacDonald, M. A.; Ridley, T. *J. Chem. Phys.* **1989**, *91*, 7355.
(41) Brand, J. C. D.; Hoy, A. R.; Kalkar, A. K.; Yamashita, A. B. *J. Mol. Spectrosc.* **1982**, *95*, 350.
(42) King, G. W.; Littlewood, I. M.; Robins, J. R. *Chem. Phys.* **1981**, *56*, 145.
(43) Hickmann, J. S.; de Olivera, C. R. M.; Francke, R. E. *J. Mol. Spectroc.* **1988**, *127*, 556.
(44) Sension, R.; Strauss, H. *J. Chem. Phys.* **1986**, *85*, 3791.
(45) Fei, S.; Zheng, X.; Heaven, M. C.; Tellinghuisen, J. *J. Chem. Phys.* **1992**, *97*, 6057.
(46) Macler, M.; Heaven, M. C. *Chem. Phys.* **1991**, *151*, 219.
(47) Bell, R. P. *Trans. Faraday Soc.* **1931**, *27*, 797.
(48) Onsager, L. *J. Am. Chem. Soc.* **1936**, *58*, 1486.
(49) Böttcher, C. J. F. *Theory of Electric Polarization*; Elsevier: Amsterdam, 1973.
(50) Vidal, D.; Lallemand, M. *J. Chem. Phys.* **1976**, *64*, 4293.
(51) Tellinghuisen, J. *J. Chem. Phys.* **1973**, *58*, 2821.
(52) Holmes, A. J.; Lawley, K. P.; Ridley, T.; Donovan, R. J.; Langridge-Smith, P. R. *J. Chem. Soc., Faraday Trans.* **1991**, *87*, 15.
(53) Heemann, U.; Knöckel, H.; Tiemann, E. *Chem. Phys. Lett.* **1982**, *90*, 350.
(54) Brand, J. C. D. *J. Mol. Spectrosc.* **1982**, *95*, 350.
(55) Brand, J. C. D.; Hoy, A. R. *Can. J. Phys.* **1982**, *60*, 1209.
(56) Steinfeld, J. I.; Klemperer, W. *J. Chem. Phys.* **1965**, *42*, 3475.
(57) Steinfeld, J. I. *Acc. Chem. Res.* **1970**, *3*, 313.
(58) Zewail, A. H. *Acc. Chem. Res.* **1980**, *13*, 360.
(59) Xu, J.; Schwentner, N.; Chergui, M. *J. Chem. Phys.* **1994**, *101*, 7381.
(60) Scherer, N. F.; Ziegler, L. D.; Fleming, G. R. *J. Chem. Phys.* **1992**, *96*, 5544.
(61) Scherer, N. F.; Jonas, D. M.; Fleming, G. R. *J. Chem. Phys.* **1993**, *99*, 153.
(62) Capelle, G. A.; Broida, H. P. *J. Chem. Phys.* **1973**, *58*, 4212.
(63) Franck, J. *Trans. Faraday Soc.* **1925**, *21*, 536.
(64) Mulliken, R. S. *Chem. Phys.* **1971**, *55*, 309.
(65) Tellinghuisen, J. *J. Mol. Spectrosc.* **1984**, *103*, 455.
(66) Felker, P. M.; Zewail, A. H. *Adv. Chem. Phys.* **1988**, *70*, 265.
(67) Materny, A.; Kiefer, W. *J. Chem. Phys.* **1992**, *97*, 841.
(68) Paige, M. E.; Harris, C. B. *Chem. Phys.* **1990**, *149*, 37.
(69) Harris, A. L.; Brown, J. K.; Harris, C. B. *Annu. Rev. Phys. Chem.* **1988**, *39*, 341.
(70) Collins, F. C.; Kimball, G. E. *J. Colloid Sci.* **1949**, *4*, 425.
(71) Liu, Q.; Wang, J.-K.; Zewail, A. H. *Nature* **1993**, *364*, 427.
(72) Potter, E. D.; Liu, Q.; Zewail, A. H. *Chem. Phys. Lett.* **1992**, *200*, 605.
(73) Wang, J.-K.; Liu, Q.; Zewail, A. H. *J. Phys. Chem.* **1995**, *99*, 11309.
(74) Liu, Q.; Wang, J.-K.; Zewail, A. H. *J. Phys. Chem.* **1995**, *99*, 11321.
(75) Zadoyan, R.; Li, Z.; Ashjian, P.; Martens, C. C.; Apkarian, V. A. *Chem. Phys. Lett.* **1994**, *218*, 504.
(76) Zadoyan, R.; Li, Z.; Martens, C. C.; Apkarian, V. A. *J. Chem. Phys.* **1994**, *101*, 6648.
(77) Li, Z.; Zadoyan, R.; Apkarian, V. A.; Martens, C. C. *J. Phys. Chem.* **1995**, *99*, 7453.
(78) Berg, M.; Harris, A. L.; Harris, C. B. *J. Chem. Phys.* **1986**, *84*, 788.
(79) Zewail, A. H.; Dantus, M.; Bowman, R. M.; Mokthari, A. *J. Photochem. Photobiol. A* **1992**, *62*, 301.

JP9624313